INVESTIGATION OF MICROWAVE TRANSDUCERS FOR LINEARITY DEPENDENCE AND APPLICATIONS IN QUANTUM NETWORKING

by

SUMMER ALEXIS BOLTON

SEONGSIN M. KIM, COMMITTEE CHAIR
PATRICK KUNG
JOSEPH M LUKENS

A THESIS

Submitted in partial fulfillment of the requirements
for the degree of Master of Science in the
Department of Electrical Engineering
in the Graduate School of
The University of Alabama

TUSCALOOSA, ALABAMA

2022

ABSTRACT

Quantum devices have the potential to revolutionize applications in computing, communications, and sensing; however, current state-of-art resources must operate at extremely low temperatures. There is an increasing interest in optical fiber transduction to microwave link with superconducting and Si qubits. The quality depends strongly on the characteristics of the photodiode, specifically modified uni-traveling carrier photodiodes (MUTC-PDs) for high-frequency operation, yet most do not have the high-speed and high-linearity performance or the ability to handle ultracold temperatures. To address these low-temperature and high-frequency problems, an RF photonic microwave transducer is used to measure the frequency response and investigate the linearity dependence on frequency, bias voltage, and temperature.

An electro-optical microwave transducer is created using the heterodyning beat method. A high-speed MUTC photodiode designed for cryogenic temperatures is tested as the transducer and characterized with a spectrum analyzer. The linearity of the device is also tested at bias voltages of 0V and −5V, frequencies of 3 GHz and 10 GHz, and temperatures of 300 K and 77K.

With a low bias voltage, the frequency response shows a decrease in power due to the increase of harmonic noise. The results show that the linearity does depend on frequency, bias voltage, and temperature. A higher reverse bias voltage showed the highest 1-dB compression point, while a bias voltage of 0 V and a frequency of 10 GHz showed the lowest power and the lowest 1-dB compression point. Our results should help contribute to the future design of highly linear cryogenic quantum links.

DEDICATION

This thesis is dedicated to everyone who supported me throughout my academic career. I would especially like to recognize my parents for their unconditional support and my close friends for joining me on this journey.

LIST OF ABBREVIATIONS

UTC-PD	Uni-traveling carrier photodiode
MUTC-PD	Modified uni-traveling carrier photodiode
PIN-PD	Positive-intrinsic-negative photodiode
THz	Tera-hertz (10E12)
MHz	Mega-hertz(10E6)
GHz	Giga-hertz(10E9)
dB	Decibels
dBm	Decibel-milliwatt
RF	Radiofrequency
ε	Permittivity of dielectric
d	Diode active thickness
A	Diode active area
hv	Photon energy: Planck's constant times the frequency of light
η	Quantum Efficiency
t_{DRIFT}	Charge collection time of carriers in the depletion region of a photodiode
$t_{DIFFUSED}$	Charge collection time of carriers in the undepleted region of a photodiode
t_{RC}	Resistor-capacitor time constant of the diode-circuit combination
ω	Angular frequency
φ	Phase

ACKNOWLEDGMENTS

This research would not have been possible without the support of my friends, fellow colleagues, and professors who have taught and encouraged me throughout this project. I express my utmost gratitude to my advisor, Dr. Seongsin M. Kim. While my undergraduate record did not indicate a strong candidate for graduate school, she saw my passion and strong work ethic, and decided to give me a chance to redeem myself. Thanks to Dr. Kim's faith and guidance I have completed this research, obtained a master's degree, and received a great job offer due to the experiences she has given me. I want to also thank Dr. Kung for the direction and support throughout my time in graduate school. Without the guidance and confidence of these two professors, I would never have gained this experience, found topics I am passionate about, or redeemed myself from being an undergraduate student without direction.

I would also like to thank Dr. Lukens at Oak Ridge National Laboratory for his collaboration and support in this project. The technical guidance and weekly meetings were crucial to the success of this research. Also, the opportunity to visit his laboratory to see the campus and use equipment to conduct my experiments. Finally, I want to thank my family and friends for the support throughout my time in graduate school.

CONTENTS

LIST OF TABLES

LIST OF FIGURES

CHAPTER 1. INTRODUCTION

1.1 Motivation

Quantum computers are the newest emerging technology in the world of computing. They allow faster and larger data transfers than the classical computers used today. Classical computers operate in a binary system, meaning a value can be 0 or 1. A string of these bits can be created and interpreted, therefore creating, and sending information. Quantum computers use a qubit, which can be 0, 1, or a superposition of both. This in principle allows more data to be processed more efficiently than possible with classical resources. While quantum computers have been prototyped and are being researched, there are a few roadblocks that prevent them from being prevalent in everyday life: they require stringent environmental conditions and highly advanced optical devices. The qubits have a very low range of energy between the quantum states, so they require ultra-low temperature, almost 0K, to introduce less energy into the system for accurate readings of the qubit. To achieve such cold temperatures presently, a small space must be vacuumed and cooled, which prevents scalability beyond a small network. Therefore, the ultra-low temperature requirements and the lack of space available in these cold temperatures are two reasons why quantum computers are not sustainable today.

Along with the environmental restraints, the devices in these systems need to be low noise, accurate, and high speed. For photodetectors, a low dark current, high responsivity, and high speed are essential to improving the scalability of quantum computing. Linearity is also an important metric for a quantum system. Having a linear device means the output power is a

scaled replica of the input optical power, which ensures an accurate electrical response and low signal distortion. Trusting a device to provide accurate and reliable data is an important feature in an optical device.

Investigating a high frequency microwave signal using analog photonic link could potentially bring quantum computers closer to being available in every household. While a higher frequency can create more noise, this can be solved by also investigating the capabilities of high speed modified uni-traveling carrier photodiodes and the linearity dependence on frequency, bias voltage, and temperature. The novelty of these investigations can provide insight and possible improvements to quantum computing systems.

1.2 Outline of Thesis

This thesis investigates multiple parameters to expand the range of quantum computers. The focus of this thesis is the characterization of a cryo-hardened MUTC photodiode with a focus on frequency response and linearity dependence at room temperature and low temperatures of 80K. It is organized as follows: Chapter 2 provides the reader with necessary background information on telecommunication and optical devices; In Chapter 3 the fundamentals of photodiodes are discussed; Chapter 4 describes the experimental setup and procedure; Chapter 5 presents the results and discusses the importance; Conclusions and future work are explored in Chapter 6.

CHAPTER 2. MICROWAVE PHOTONIC LINK

2.1 History of Telecommunication

Optical communication, which in general is communication by use of light, dates back thousands of years. Civilizations used light when sound wasn't enough by using mirrors to reflect light, fire beacons, and smoke signals to convey victory or signs of help. Common issues with using fire and light are the available distance that can be seen with the naked eye and visual blockages such as fog and rain.

In 1792 Claude Chappe developed the first practical telecommunication system of the industrial age which he called the optical telegraph, also known as the semaphore system. The alphabet was coded by the position of two needles and a neighboring tower used a telescope to read and pass the message, essentially acting as a repeater. Light was used to see the other towers, but this process was slower than 1 bit/s per kilometer traveled. This method of communication was used until the 1830s when the electrical telegraph was developed [1]. After the discovery of electricity, electrical communication dominated and optical communication development was disregarded. Morse code allowed communication over large distances by electrical pulses of two different sizes to represent dots and dashes. This code increased the speed of data transmission to approximately 10 bits/s per kilometer. The invention of the telephone in 1876 served as the foundation for future large-scale communication and the

speed of transmission increased to approximately 1000 bits/s per kilometer. In this time, communication was still limited by distance and large transmission loss.

The invention of the coaxial cable began in the early 1900s to decrease the enormous loss in transmission. By wrapping the lines with insultation, the loss of the signal decreased and the durability of the cables increased. Speeds of approximately 1Mbits/s per kilometer were achieved with the use of coaxial cables. The bandwidth of these cables began at 3MHz and could transmit hundreds of voice channels, but as the frequency increased into the GHz range, the cable loss was too high. This loss led to the research and development of microwave communication systems with electromagnetic frequencies, which increased the bit rate distance product to approximately 10Mbits/s per kilometer using the repeater spacing as the distance [2]. After the invention of the laser in the 1960s, optical communication made a large return. At the time, optical fiber was used for making devices but only required a short distance of fiber. Optical fiber had such high losses that the estimated maximum possible distance over which it is possible to achieve 99% reliability of transmission was only a few kilometers [3]. The race to improve optical communication commenced with back-and-forth research and improvement techniques by modifying the materials used in optical fiber and improving the laser source.

2.2 Coaxial Cable vs. Optical Fiber

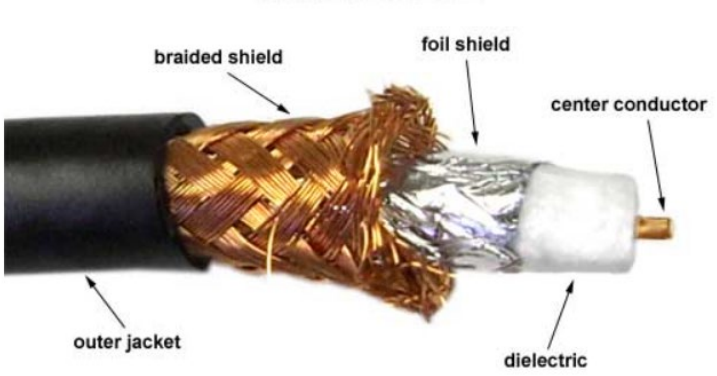

Figure 2.1 Structure of coaxial cable [4]

Coaxial cable is the traditional transmission for communication. The inner-most layer is a conductor that transmits data using electricity, commonly a copper-plated steel wire. This conductor can be solid or stranded to increase flexibility and silver plated to increase performance. The dielectric layer separates the conductor layers, typically a form of plastic or air with spacers. In lower-loss cables, polyethylene is used as the insulator. Another conductor is formed on top of the dielectric, usually a foil shield or a braided shield. Using a braided shield allows greater flexibility but allows gaps in the layer and the inner dimension will vary because it cannot lay completely flat [4]. Cables will often have a double layer shield to improve performance; however, the more shielding that is used, the decrease in bend radius available. The outer jacket protects the cable inside and increases durability and can be made from many materials, commonly PVC or fire-resistant material. Having an insulation layer decreases the energy loss and decreases the chance of crosstalk with neighboring cables. Each layer size and material affects the performance, loss, and attenuation of the cable [5]. Coaxial cables are quickly being replaced by a faster method of transmission: the fiber-optic cable.

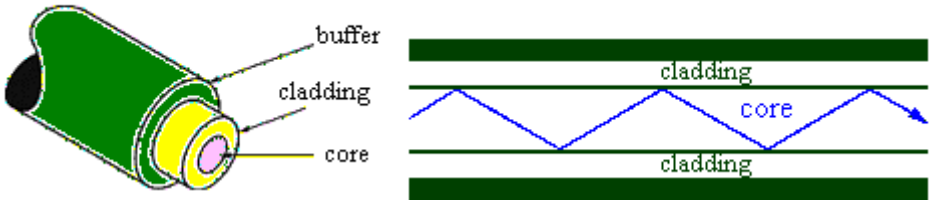

Figure 2.2 Structure of fiber-optic cable(left) and passage of light through core(right) [6]

Fiber-optic cables are made of glass fibers that use light to transmit data. Optical fibers are waveguides, meaning they guide the photons by constraining a path for it to follow. The innermost layer is the core and it carries the light. Outside of the core is the cladding which helps constrain the light so it follows the path. The cladding layer has a lower refractive index than the core, causing the light to zigzag between the two mediums, also known as total internal reflection. This allows the light to travel inside the core without exiting the fiber. Often a buffer or jacket is used to protect the core and cladding layer from the physical environment. Coatings and additional layers can be added to the fiber to reduce shock, increase protection, and reduce crosstalk between the fibers [6]. Multiple fibers with a core, cladding, and buffer can be combined to form a larger fiber optic cable that transmits more data.

Optical fiber can have different properties based on refractive index, core size, numerical aperture, and material [7]. Silica core with doped or undoped silicon are used for long distance transmission. A small core size with glass as the protective coating are used in ultraviolet visible spectroscopy. The mode of propagation can also be changed by the geometry of the fiber. A small core size of 8.3-10 micrometers allows only one mode of propagation to pass, also known as single mode fiber. The core is small enough that it can isolate the beam so only one mode passes through. Within single mode fiber, there is also polarization maintaining single mode

fiber. This type of fiber has a strong internal birefringence that properly orients the beam of light. While single mode allows one mode of propagation, meaning any random polarization that is dominant can pass, polarization maintaining fiber allows the preservation of the polarization aligned to either the slow or fast axis [8]. Single mode is typically used with a laser and has a higher bandwidth than multimode. Multimode optical fiber has a larger core diameter that allows multiple modes of light to pass therefore allowing more data transmission. Allowing multiple modes of propagation is useful for larger data transmission for short distances.

Both copper coaxial cables and optical fiber have their advantages and disadvantages. Coaxial cables are cheaper and typically more durable, but optical fiber supports higher bandwidth and is less susceptible to interference [9]. Optical fibers also require a form of optical to electrical conversion to use the light as electricity, whereas no conversion is needed for coaxial cables. Figure 2.3 depicts the greatest advantage of optical fiber over coaxial cables: low loss with bandwidth and distance. Two common coaxial cables, RG-405 and RG 401, are compared against optical fiber made of silicon. The two coaxial cables have significantly greater loss than the fiber, specifically the loss increases one decade for every two magnitudes in frequency, and is at least two orders of magnitude higher than the loss in the fiber. Generally, a larger cable such as the RG-401 would have lower loss, but also has a lower cutoff frequency than the fiber. While coaxial cables appear to have lower loss than fiber at short distances, this loss arises from the optical to eletrical conversion required when using fiber optic links, so the fiber actually has negible loss. Also, the cost, performance, and immunity from interference can make optical fiber more appealing even at smaller distances [10].

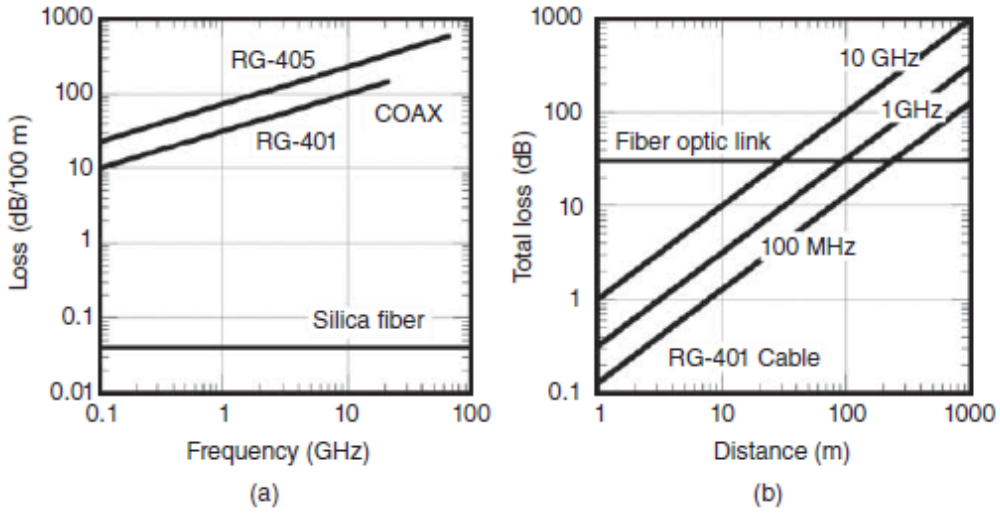

Figure 2.3 Fiber type comparison with frequency(a) and distance(b) [10]

2.3 Microwave Photonics

Microwave photonics covers many fields of engineering including optics, microwaves, and electrical engineering. Microwave electromagnetic frequencies can cover 1MHz to 100GHz, which corresponds to wavelengths in radio and infrared waves. Microwave technology is used in a variety of sensing and imaging applications including satellites, radar, security, and medical systems [11]. Due to the broad bandwidth available and high transmission rates, microwave technology is also used in wireless networks and will likely prove useful in quantum networking. This frequency range is ideal for communication because the microwave wavelength is longer than visible and infrared light, so it can easily penetrate through many environmental conditions such as rain, fog, and clouds. There is a demand for the generation of microwave signals for high-speed and high-power applications, but the current devices available as sources are limited by the low power output and high phase noise. Photonic microwave signal generation can fix some of the limitations that electrical generation cannot provide [12].

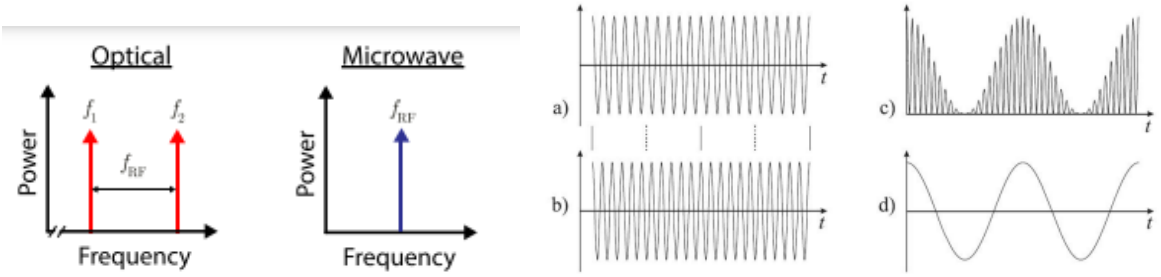

(a) (b)

Figure 2.4 Concept of photo mixing in frequency domain (a) and time domain (b) [14,15]

Photonic microwave signal generation can provide higher bandwidth, low loss, and higher data transmission rates when compared to the coaxial cable. Transmission of a microwave signal via electrical circuitry requires many stages of frequency doubling and introduces high loss over large distances due to using coaxial cables [13]. The optical generation of microwave signals is created with the beating of two optical waves through a high-speed photodetector. A basic diagram of the photo mixing process is shown in Figure 2.4. Two different optical wave sources are combined with a coupler, sent through a photodiode, and the output is a microwave signal equal to the difference of the two frequencies [14]. The input versus output is also shown in Figure 2.4(b). In the frequency domain, two optical sources are combined to form one frequency in the microwave regime. In the time domain, two waves with slightly different frequencies, pass through a fast photodiode and create the squared sum of the signals, also the beat note shown in Figure 2.4(right) [15]. It can be further explained in equations 2.1 through 2.3. Two optical waves described with amplitude E_{01} and E_{02}, angular frequencies of ω_1 and ω_2, and phase of φ_1 and φ_2, beat at the photodetector and produce a single electrical current determined by the amplitudes of the two lasers and the responsivity of the photodetector [13].

$$E_1(t) = E_{01}\cos(\omega_1 t + \varphi_1) \tag{2.1}$$

$$E_2(t) = E_{02}\cos(\omega_2 t + \varphi_2) \tag{2.2}$$

$$I = \mathrm{Acos}[(\omega_1 - \omega_2) + (\varphi_1 - \varphi_2)] \tag{2.3}$$

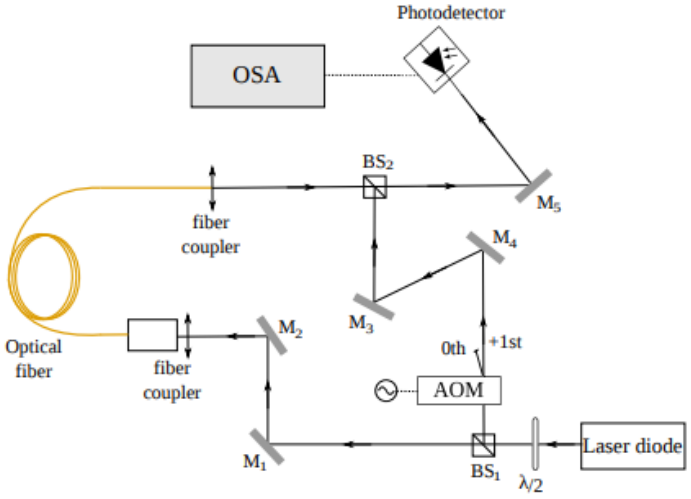

Figure 2.5 Experimental setup of delayed self-heterodyne technique [15]

The generation of the two sources can be done with a single laser source that is then externally modulated and recombined, shown in Figure 2.5. This diagram shows the delayed self-heterodyne technique. The laser diode source is split with one path going through mirrors and coupled to optical fiber, the other is modulated using a frequency shifter. Both beams are recombined and directed to the photodetector and the optical spectrum analyzer. The use of mirrors allows the beam to be directed and free space allows a delay in the transmission [15].

Another popular technique for microwave optical signal generation is the heterodyne technique with two separate laser sources, with a general diagram shown in Figure 2.6. Two

separate lasers with different frequencies are combined, passed through a fast photodiode, and the result is an RF signal with the frequency being the difference in the two lasers. If one of the laser sources is independently tunable, the only limitation is the bandwidth of the photodetector. Under this restriction, any microwave wavelength can be reached with a large enough separation of the laser frequencies [16].

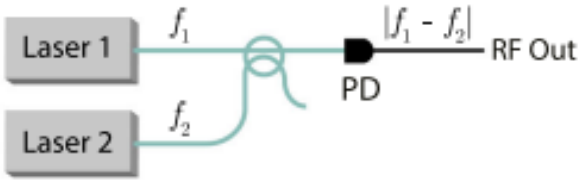

Figure 2.6 Diagram of heterodyne method with two independent laser sources [16]

For the optical heterodyne technique to be efficient in microwave signal generation, the optical power and polarization must be equal. Otherwise, the resulting tone after the detector will have less amplification than desired. The sum of the optical powers and the difference in frequency can be achieved to produce 100% modulation efficiency, but a slight difference in power or polarization could cause instability in the measurement. Optical devices are often used as filters to preserve the desired polarization and aid in a large modulation efficiency. A polarization controller is used to filter the desired state of polarization of an incoming light wave [17]. The controller works by applying pressure on the optical fiber, causing a birefringence within the fiber core. Changing the pressure changes the delay of the polarization components, while rotating the direction of stress allows any polarization to be achieved. The polarization of light can also be filtered with an in-line polarizer. A polarizer allows linearly polarized light to pass through while blocking the randomly polarized light source, shown in Figure 2.7. Only a

specific orientation of light can pass through the polarizer depending on the filter used. These components for controlling and filtering the polarization of light allow two lasers to have the same polarization, allowing a stronger signal when detected [18].

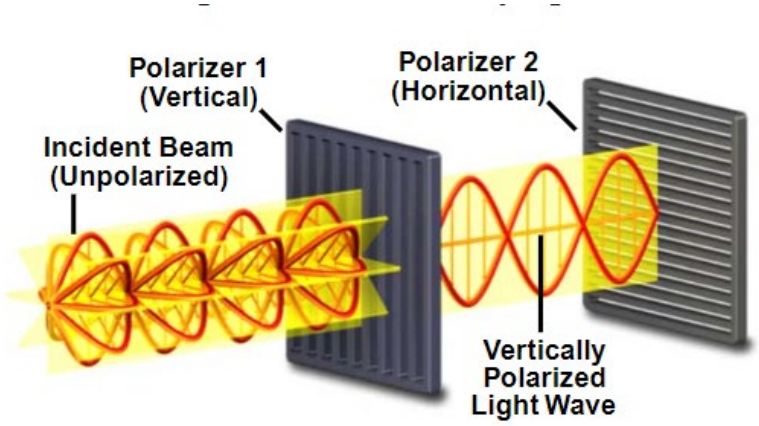

Figure 2.7 Polarizer as a filter [18]

Once the two lasers have the same optical power and polarization, they can be combined using a coupler. A fiber optic coupler can split the signal from one fiber into two or combine the signal from two fibers into one. Couplers come in many configurations, but this experiment uses a 2x2 wideband single mode fiber coupler with a 50:50 split. This means the coupler has two inputs and two outputs; it combines the signal into one and splits the signal evenly between the two outputs, so each output receives half the combined signal. Inside the coupler, the cores of the fibers are fused together to combine the signal. The coupler can produce significant coupling loss if it is single mode unless the inputs are mutually coherent. This further emphasizes the importance of equal power and polarization of the two laser sources.

CHAPTER 3. PHOTODIODE FUNDAMENTALS

Photodetectors are devices used in the detection of light that convert an input optical power to an output electrical signal. Photodiodes are semiconductor devices that fall under the category of photodetectors and are commonly used in optical communications. Different types of photodiodes provide different advantages and properties depending on the application. The properties and types of photodiodes are discussed in this section.

The basis for the first photodiode began with a modified lightbulb in the early 20th century. Thomas Edison discovered that when an extra electrode was added in a light bulb and connected to the positive side of a battery, the current flowed through the filament through empty space. G.W. Pickard continued this and experimented with the idea that electricity will only flow in one direction through certain types of crystals. Pickard made the first cat-whisker diode by placing silicon crystal between a metal base and carefully placed wire. This diode was widely used for detection in radios, but the fragility of the alignment made these devices hard to use [19]. Over time more research was conducted on materials and semiconductor devices, leading to advancements such as the positive-intrinsic-negative (PIN) diode, the uni-traveling carrier (UTC) photodiode, and the modified uni-traveling carrier photodiode (MUTC).

The formation of a diode begins with the material: semiconductors. Semiconductors are not conductors or insulators; they have a few free electrons because their atoms are grouped to form a crystal lattice, but the electrons will only flow under certain conditions. The most

common materials for semiconductors are Silicon and Germanium, but the total number of valence electrons must equal 8, so multiple materials can be used. A p-type semiconductor is formed when two atoms are bonded but are missing one electron; this missing electron is called a hole. The neighboring electron is attracted to this hole and moves to fill the space, so the material is accepting an atom; however, the neighboring atom has lost an electron, creating a hole. Another neighboring electron moves to fill this space, and the cycle repeats. This is shown in Figure 3.1. Boron has 3 valence electrons and Silicon has 4. These two elements form a covalent bond, but still have a space for an electron. This forms a p-type semiconductor because there are more holes than electrons.

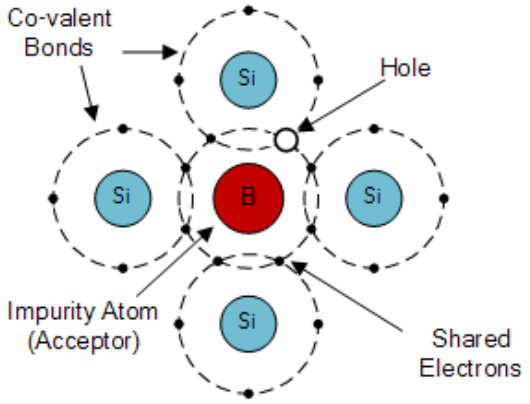

Figure 3.1 P-type semiconductor doping [20]

A similar process occurs in n-type semiconductors which are formed when two atoms are bonded but have an extra electron, or a donor electron to give. The free electron becomes mobile when stimulated by a voltage source, but is replaced by the other electrons, resulting in having a free electron again. An example is shown in Figure 3.2 with Antimony and Silicon. Antimony has 5 valence electrons and Silicon has 4. These two atoms form covalent bonds, but Antimony

has a free electron. When stimulated, this free electron will move but be replaced by the other electron [20]. This results in more electrons than holes, so electrons are the majority carriers, and created an n-type semiconductor.

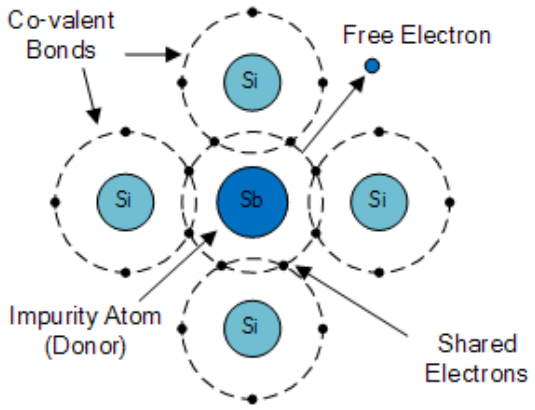

Figure 3.2 N-type semiconductor doping [20]

Different materials used in semiconductors provide different properties such as dark current, wavelength, speed, and sensitivity. Doping, or the process of combing two atoms to produce a hole or an electron, can also change the electrical characteristics of the semiconductor. Material properties change depending on the position on the periodic table, so III-IV semiconductor materials will behave differently than II-VI materials. While elements, such as Silicon, can be used alone in a diode, using compound materials can change and enhance certain characteristics. In the past, these compound materials were hard to produce due to the difficulty of crystal growth and fragility; however, the cost of manufacturing has decreased and these materials provide properties that elemental materials cannot [21]. Table 3.1 below shows some common materials for diodes and some characteristics of each [22].

Table 3.1 Properties for common photodiode materials

Material	Wavelength	Dark Current	Speed
Silicon (Si)	400nm-1000nm	Low	High
Germanium (Ge)	900nm-1600nm	High	Slow
Indium Gallium Arsenide (InGaAs)	900nm-1700nm	Low	High

In summary, a diode is a device that allows current to flow in only one direction. Two semiconductor materials are combined and doped to create a positive p-type region with holes as the majority characters and a negative n-type region with electrons as the majority carriers. The characteristics of the diode are initially determined by the material and further changed by the levels of doping in the material. While the first diode was simply formed from the discovery of the lightbulb, many advances have been made to make diodes one of the most common electronic devices.

3.1 Photodetector Parameters

The characteristics of the photodiode are largely determined in the fabrication process. Changing the material, structure, and doping levels will affect the performance of the diode. Especially for the long wavelength infrared region and the mid wavelength infrared region, there is not a one size fits all photodiode. Different applications may require higher frequencies at the cost of lower performance, and some may desire high speed at the cost of saturation current. Important parameters to characterize the performance of a photodiode are bandwidth, responsivity, and quantum efficiency.

3.1.1 Bandwidth

Frequency response describes the speed of a photodiode. As the optical frequency increases, at some point the RF power decreases. The 3dB bandwidth is the frequency at which the RF output power drops by 3dB, which is 50 percent of the initial power. The frequency where the photodiode begins to decrease in power is mainly determined by three factors: the charge collection time of carriers in the depletion region, t_{DRIFT}, the charge collection time of carriers in the undepleted region, $t_{DIFFUSED}$, and the RC constant, t_{RC}. The RC limited bandwidth is defined in equation 3.1 with *d* being the thickness of the active layer and *A* is the device area. This limitation stems from the photodiode acting as a junction capacitance in parallel with the junction resistance, which are parallel to the series resistance and load resistance in series. Increasing the depletion width will decrease the capacitance and increase the bandwidth; however, this will lead to a larger transit time and a smaller transit time limited bandwidth [10].

$$f_{3dB} = \frac{1}{RC} = \frac{d}{\varepsilon AR} \tag{3.1}$$

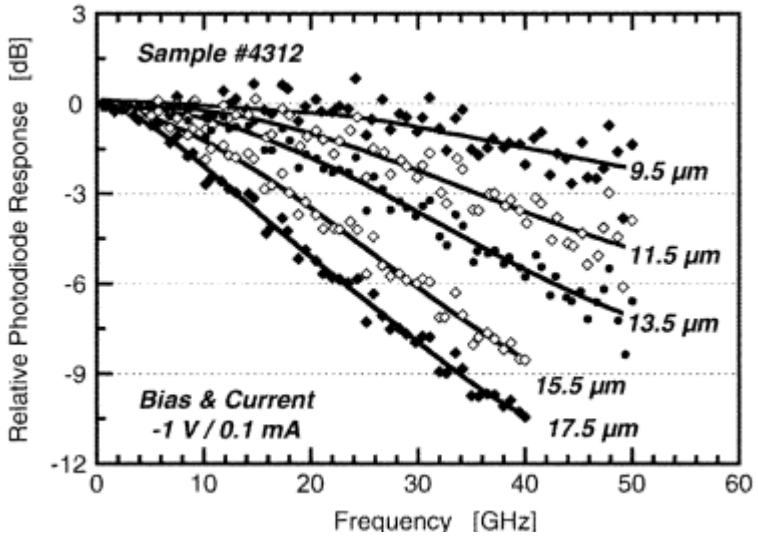

Figure 3.3 Frequency Response of UTC-PD with changing photodiode diameters [23]

The UTC-PD has a faster response than the PIN-PD due to only allowing the fast electrons into the collection layer, so the determining factor of the bandwidth derives from the electron diffusion through the absorption layer. Shown in Figure 3.3, the size of the photodiode diameter largely determines the frequency response. The results of larger area photodiodes are limited by the RC-limited bandwidth and the carrier transit time limited bandwidth [23]. Frequency response is typically measured using two techniques: intensity modulator or optical heterodyne. In the first method, a laser drives a Mach-Zehnder modulator (MZM) and is amplified by an EDFA then attached to a photodiode. The RF power can be measured using a power meter or the signal is connected to a vector network analyzer. Advantages of this method are high resolution at low frequency; however, the bandwidth is limited by the modulator and the components used. The other method is the optical heterodyne method, discussed in Chapter 2. With the optical heterodyne method, two lasers are combined so the beat frequency between them is equal to the modulation frequency after the photodiode. The advantages of the

heterodyne method are high tunability since the individual laser frequencies can be changed; however, the precision of the modulation efficiency can decrease with a large frequency offset.

3.1.2 Responsivity

Responsivity measures the photodiode's sensitivity of light, defined as the ratio of photocurrent to the incident light power at a given wavelength:

$$R_p = \frac{I - I_{dark}}{P} \tag{3.2}$$

where P is the input optical power, I-I_{dark} is the photocurrent. This parameter measures how effectively the diode can convert optical power into electrical current. Although not shown in the equation, responsivity does vary with wavelength, bias voltage, and temperature [24].

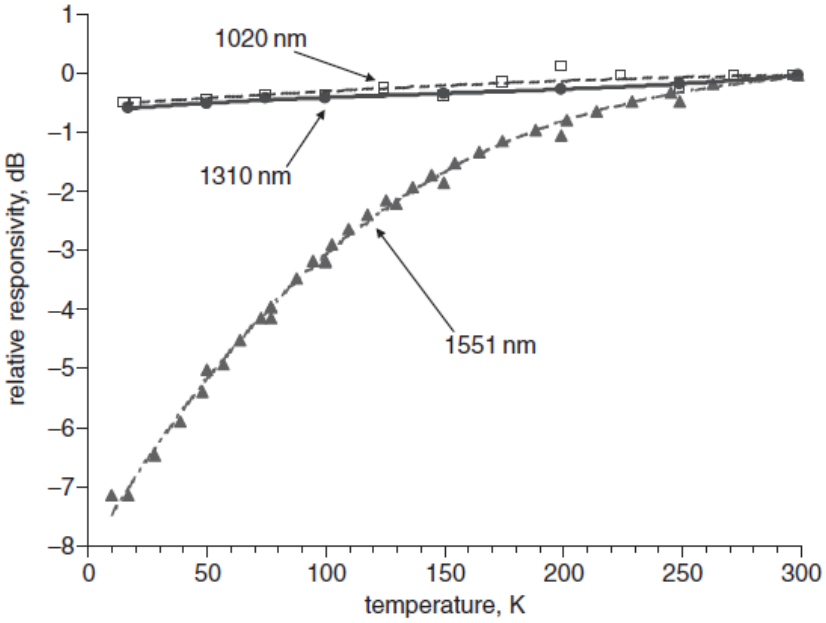

Figure 3.4 Relative responsivity vs. temperature for different wavelengths [25]

Responsivity changes with wavelength and temperature but scales linearly with input optical power. Figure 3.4 shows the temperature dependence of responsivity for a UTC-PD. While the lower wavelengths are mostly unaffected, the results with a wavelength of 1551nm shows a decrease in responsivity at lower temperatures [24]. As temperature decreases, the energy of the electron decreases, so they are slower to move between energy bands and slowly approach carrier freezeout.

Responsivity is closely related to external quantum efficiency, which describes how effectively a device converts incident photons into electron-hole pairs that contributes to photocurrent. Responsivity is the external quantum efficiency times the elementary charge, e, divided by the photon energy, hv.

$$R = \eta \frac{e}{hv} \tag{3.3}$$

Quantum efficiency is determined by the reflectivity of the surface, the absorption layer thickness, and the absorption coefficient of the material. Shown in Figure 3.5, different materials also exhibit different responsivities and quantum efficiencies with different wavelengths. It is shown that InGaAs has a large responsivity and a quantum efficiency of approximately 60% for wavelengths around 1550nm. Different materials have different responsivities and quantum efficiencies for different desired wavelengths [26].

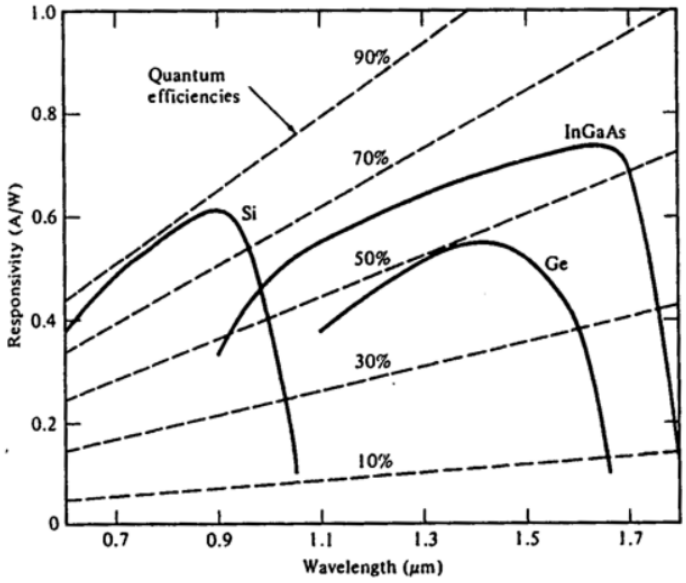

Figure 3.5 Responsivity vs. wavelength for semiconductor materials [26]

3.1.3 Linearity

A photodiode is considered linear when the photocurrent increases linearly with RF power. Linearity is an important parameter because it ensures an accurate electrical response without reaching saturation current. The need for high power and high linearity devices arises for application in microwave photonics and antenna imaging [27].

Linearity can be defined by a compression curve with a 1dB compression point (P1dB), the third intercept point (IP3, OIP3). The P1dB is defined as the RF power which causes the conversion loss to increase by 1dB. This metric can be found using Figure 3.6 as an example. In a plot showing measurement results with power output versus power input, the P1dB is found when the gain is 1dB below the ideal or theoretical response. Another method is to create a compression curve, which shows the measurement results subtracted by the ideal response. The P1dB is found 1dBm below the peak value on a compression curve.

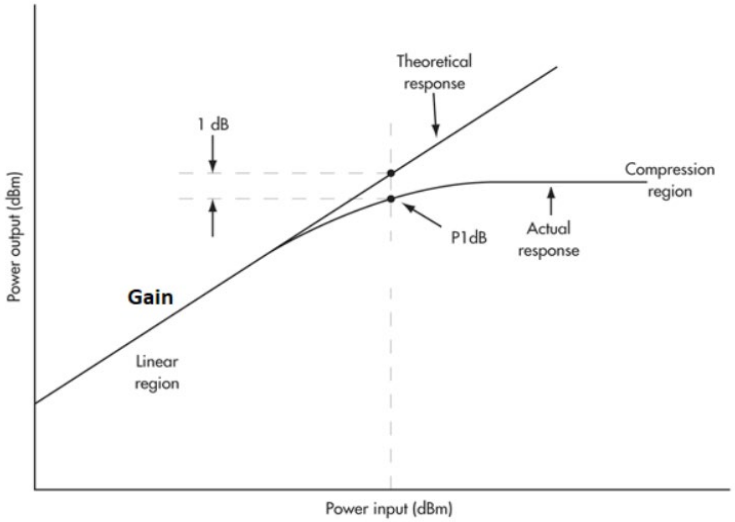

Figure 3.6 Diagram of P1dB

Another important linearity metric is the IP3 or OIP3. Typically, a two-tone setup is used to find the OIP3. Two independent laser sources are sent into their own modulators, essentially have four initial tones. After a high-speed photodiode, only two tones appear with their harmonic distortions. The fundamental signal is the largest peak, then the third and second order points arise from the second and third order harmonics. These results are plotted on the same graph and the output power where the fundamental frequency, theoretically, would intercept the third order distortion is the OIP3. The IP3 is the input power where the fundamental response would theoretically intercept the third order response [28].

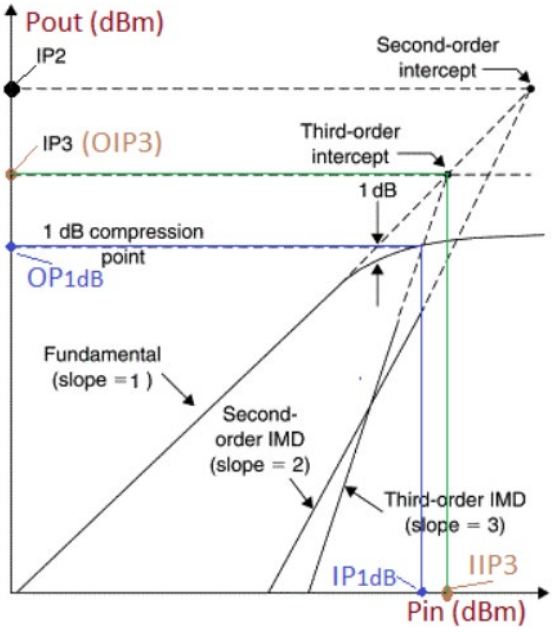

Figure 3.7 Diagram of OIP3 concept [28]

3.1.4 Limitations

Photodiode characteristics are determined by many factors including structure, material, temperature, and applied bias voltage. While photodiodes can be tuned to have higher performance or higher bandwidth, there are tradeoffs when choosing the characteristics of the photodiode. Doping and material largely affect the characteristics but there are two main limitations to photodiodes that can be altered but not avoided: the space charge effect and carrier freezeout.

First important limitation is the space charge effect. Typically, photons with a higher energy will be absorbed which creates electrons and holes, then electrons diffuse to the n-doped region and holes diffuse to the p-doped region. When there is high optical power, the excess carriers have high density near the p and n regions, which creates an electric field that opposes the field produced by an applied bias voltage. This collapse in the field creates a lower

bandwidth and saturation of the RF power [29]. Space charge effect is determined by the diode size, structure, illumination conditions, etc. The effect can be reduced by increasing the bias voltage but doing so can increase risk of electrical breakdown of the diode.

Another important limitation is carrier freezeout when a photodetector is operated at low temperatures. At low temperatures, the dopants don't have enough energy to ionize and produce carriers. With the appropriate doping levels according to the semiconductor material and doping type, the temperature at which carrier freezeout occurs can be reduced [30]. This is shown in Figure 3.8 comparing the band gap energy versus temperature for different materials. At low temperatures the energy between the conduction band and valence band increases, meaning it takes more energy to excite a photon. [22].

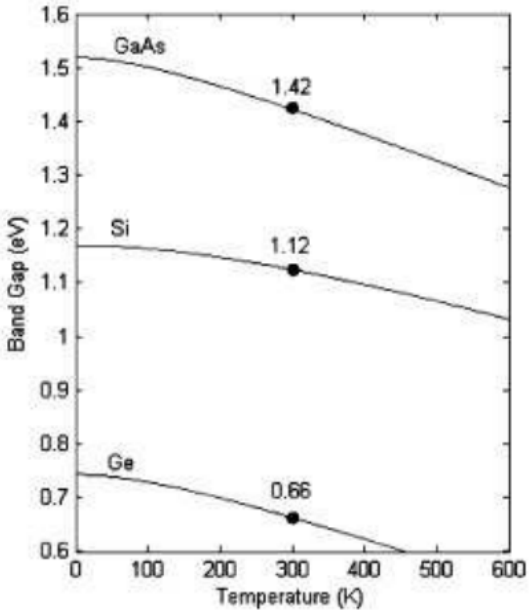

Figure 3.8 Temperature dependence of band gap [22]

While these limitations are unavoidable and can cause problems, measures can be taken to reduce these effects. Choosing the right temperature, structure, and doping levels can provide

a photodetector that matches the needs of the application. With these parameters and limitations in mind, the structures of the photodiode can also affect characteristics of the performance.

3.2 PN Diode

The PN diode, or junction, is the basic structure of a diode, but the theory applies to more advanced diodes as well. An n-type semiconductor is fused with a p-type semiconductor to form a PN junction. When combined, the free electrons from the n-type region travel across the junction to fill the holes in the p-type region, leaving one side full of positively charged donor ions and the other with negatively charged acceptor ions, as shown in Figure 3.9.

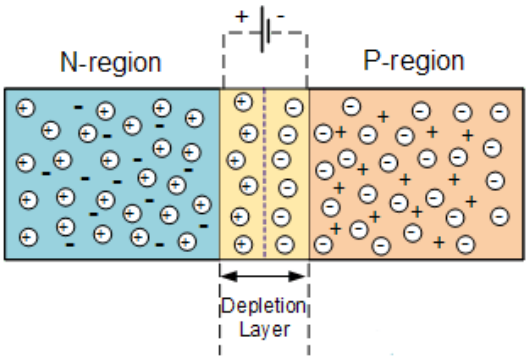

Figure 3.9 PN junction structure [20]

While this diffusion is occurring, an electric field is formed in the depletion region as described in the equation below. The electric field created by diffusion at zero bias voltage is described as the thermal voltage times the ratio of number of acceptor ions times the number of donor ions divided by the intrinsic concentration squared. This occurs even with no external applied voltage, which is why dark current is prevalent in diodes.

$$E_o = V_T * \ln \frac{N_A * N_D}{n_i^2} \tag{3.4}$$

A PN diode is a PN junction with a terminal voltage source connected to the p-region and the other terminal connected to the n-region. Applying a voltage overcomes the potential barrier of the junction while in equilibrium and allows current to flow in one direction. Changing the terminal connections to each side of the diode changes the characteristics of the diode.

Reverse bias occurs when a positive voltage is applied to the n-type region and a negative voltage is applied to the p-type region, as shown in Figure 3.10a. This voltage causes electrons from the n-region to move towards the positive side and holes in the p-region to move toward the negative side. The depletion region grows and acts as an insulator due to high impedance, and a high potential barrier is created across the junction. Increasing the depletion width means majority carriers cannot carry current, but the minority carriers are able to; however, this current is very small and considered negligible.

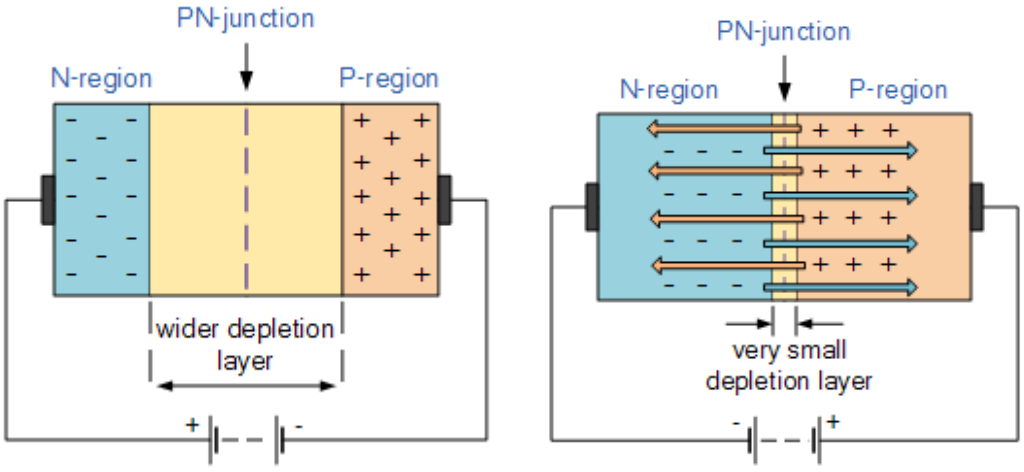

(a) (b)

Figure 3.10 Depletion width size change due to reverse bias (a) and forward bias (b) [20]

Forward bias occurs when a negative voltage is applied to the n-region and a positive voltage is connected to the p-region, shown in Figure 3.10b. The negative terminal repels electrons towards the junction and the positive terminal pushes holes towards the junction as well, causing high current to flow after overcoming the threshold voltage.

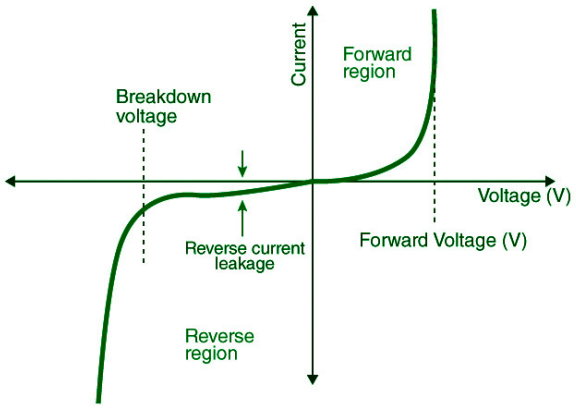

Figure 3.11 Current-voltage characteristics with varying bias voltage

Figure 3.11 shows the I-V characteristics of the PN junction diode at reverse bias and forward bias. In reverse bias, there is a small leakage current that passes. When the breakdown voltage is reached in reverse bias, a large amount of current will flow. In forward bias, the current is small until the threshold voltage is reached, then a large flow of current passes through the device. The I-V characteristic above can be described using the diode law, or Shockley ideal diode equation.

$$i(v) = I_s \left[\exp\left(\frac{v}{n*V_T}\right) - 1\right] \tag{3.5}$$

Where I_s is the reverse saturation current, v is the bias voltage, n is the emission coefficient, and V_T is the thermal voltage. This equation is true when the bias voltage is greater

than the breakdown voltage. In reverse bias, the current is approximately equal to the saturation current. The threshold voltage for current to flow and the breakdown voltage depend on the material properties of the device [20].

The PN junction serves as a basis for more advanced diodes. By adding layers, elements, or changing doping levels, the characteristics of the photodiode can be changed or improved. More advanced structures build on the foundations explored in the simple PN diode.

3.3 PIN Diode

PIN Diode stands for positive-intrinsic-negative diode. It has a structure similar to the PN diode, but there is an intrinsic layer between the p and n doped regions. This extra layer is typically a semiconductor material that is undoped, usually silicon or germanium. The band diagram in Figure 3.12 explains the structure and functionality. Incoming light generates free electrons in the conduction band and holes in the valence band inside the intrinsic middle layer. Due to the intrinsic electric field and applied bias voltage, the electrons travel to the n-layer and the holes travel to the p-layer. Adding the intrinsic layer allows a large volume of electron-hole pairs to form. This layer increases resistance and allows the p and n-layer to be more heavily doped if desired. Since holes and electrons act as carriers, the PIN diode is faster and has a higher frequency response than the PN diode.

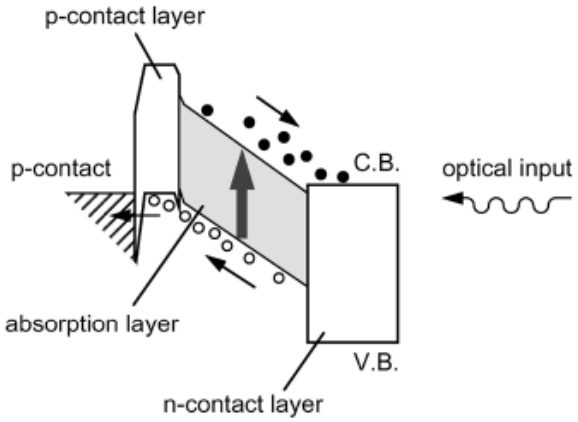

Figure 3.12 Band diagram of PIN photodiode [31]

In forward bias, PIN diodes act like a resistor in series with a parallel resistor and capacitor. While in forward bias the depletion region decreases, causing a spike in capacitance and a decrease in responsivity. In reverse bias, the diodes act as a variable capacitor. The depletion region increases and maximizes the photosensitive area for electron-hole generation. The reduction in junction capacitance decreases the RC time constant, but the transit time increases due to the carriers leaving the intrinsic region to reach the layer contact [31].

The biggest advantage of the PIN diode versus the PN diode is the added intrinsic layer. While the current-voltage curves may be similar, the addition of the depleted layer decreases the capacitance and increases the volume for electron-hole generation, which allows for a larger breakdown voltage. Compared to the PN diode, the PIN photodiode has a faster speed, higher quantum efficiency, and higher bandwidth.

3.4 UTC Photodiode

UTC Photodiode stands for uni-traveling carrier photodiode and uses electrons as active carriers. This photodiode builds off the PIN diode but adds a p-type absorber region next to the intrinsic layer. Figure 3.13 depicts the band diagram for a UTC-PD. Incoming light generates free electrons in the conduction band and holes in the valence band inside the new p-type absorber. An added blocking layer between the p-contact and the absorber prevents electrons from diffusing to the p-layer, so only electrons diffuse to the collection layer and reach the n-layer. The photogenerated holes reach the p-layer, but the cliff layer in the valence band blocks the holes from diffusing into the collection layer. This means that only fast electrons diffuse into the n-contact and holes can quickly reach the p-contact.

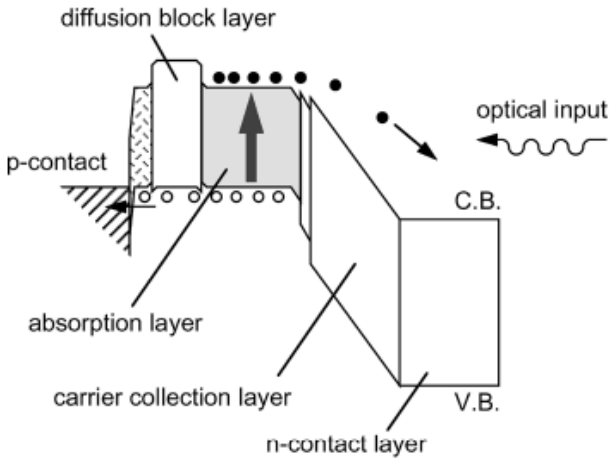

Figure 3.13 Band diagram of UTC-PD [31]

Compared to the PIN diode, the UTC-PD is faster, allows higher power, and has reduced space charge effect. Figure 3.14 shows the photoresponse of a PIN-PD (a) and a UTC-PD (b) in an output voltage versus time plot. In the PIN-PD plot, the tail of the graph to the right is due to

the slow transport time of the holes and the slow response time is due to the space charge effect [32]. The UTC PD plot shows wide linearity and fast response time.

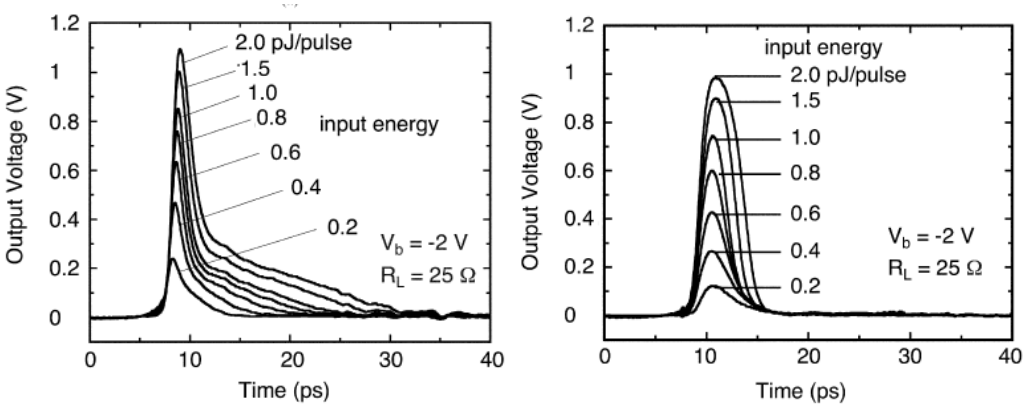

(a) (b)

Figure 3.14 Pulse photoresponse of PIN-PD (a) and UTC-PD (b) [32]

The UTC-PD has a higher speed, higher saturation current, and wider linearity than the PN-diode and the PIN-diode. Since the UTC-PD has a stronger performance in these metrics, it is often chosen in optical communication, terahertz applications, and broadband sensing [33].

3.5 MUTC Photodiode

An MUTC Photodiode is a modified uni-traveling carrier photodiode. The structure and characteristics are very similar to a UTC-PD, but an undoped layer is added between the absorption layer and the drift layer. An attempt to decrease the absorption layer thickness to reduce the carrier transit time will increase speed, but at the cost of reduced responsivity [34]. Decoupling the photon absorption from the carrier transport can keep the high speed while increasing the responsivity.

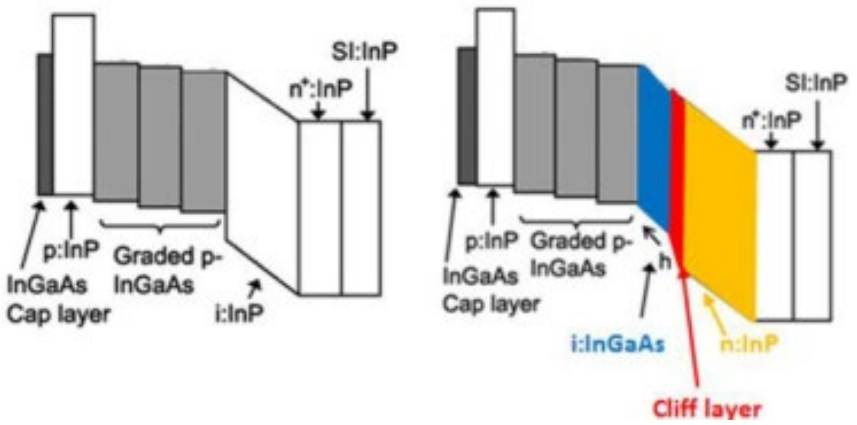

(a) (b)

Figure 3.15 Band diagram comparing UTC-PD (a) and MUTC-PD (b) [35]

Figure 3.15 demonstrates the structural differences between the UTC-PD(a) and the MUTC-PD(b). The MUTC-PD has the benefits found in the UTC-PD, but the addition of a moderately doped cliff layer between the n-contact and the absorber enhances the electric field in the depleted portion of the absorption layer. The electron drift layer, n:InP, is lightly n-type doped to compensate for high photocurrents causing a reduction in the electric field [35].

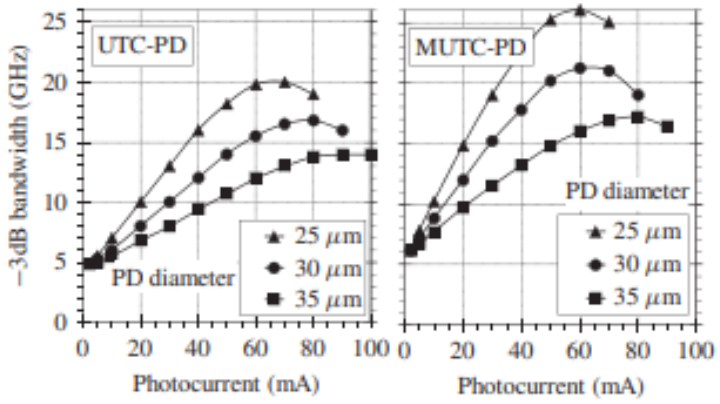

(a) (b)

Figure 3.16 Bandwidth vs. average photocurrent for UTC-PD(a) and MUTC-PD(b)

The two devices compared in Figure 3.16 have similar band diagrams, except the MUTC-PD has partially p-doped absorption layer. Both structures have a thick absorption region that results in a comparable responsivity. As shown in the figure, the MUTC-PD has a larger frequency response that is attributed to the shorter diffusion time in the thinner p-doped region and the lower junction capacitance in the thicker depletion region. While the UTC-PD reached a higher saturation current due to the electrons being the only active carriers, the MUTC-PD had a higher frequency response and higher linearity [36]. Thee added benefits and improved performance in the MUTC-PD prove it is a strong choice for high speed, high bandwidth, and high linearity applications.

CHAPTER 4. EXPERIMENTAL SETUP AND PROCEDURE

The experimental setup is designed to create an efficient transducer to convert optical energy to electrical energy and to use this transducer to characterize an MUTC-PD. Not only is the investigation of high frequency microwave signals applicable to quantum drives, but the dependency of common photodiode parameters such as responsivity, frequency response, and linearity with temperature changes can add useful insight to potential configurations for quantum systems. This chapter explains the configuration for the microwave signal and experimental setups for basic photodiode characterization, frequency response measurements, and linearity measurements. Software tools were used to alleviate human error caused by interaction with multiple instruments and stability in measurement results.

4.1 Signal Generation

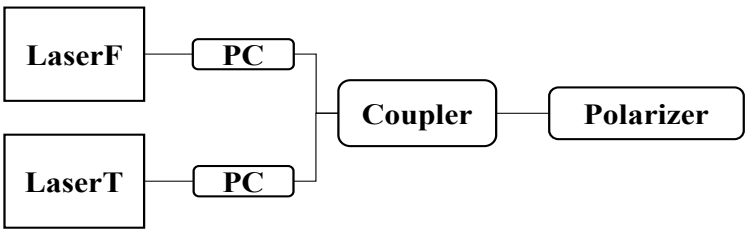

Figure 4.1 Experimental setup for heterodyne signal generation

The fundamental system is designed to create the heterodyne signal: it controls the polarization of each laser individually then combines them into one signal to ensure maximum

possible modulation efficiency. Throughout the experiment two lasers are used: one is a distributed feedback laser with a fixed wavelength dependent on current (LaserF), and the other is tunable with frequency and power (LaserT). Before any experiments can begin, the base system must be calibrated and tuned to achieve the maximum possible modulation efficiency, so the polarization and the optical power need to be matched.

First, LaserF is connected to its polarization controller and set to 140mA, the current used for frequency response measurements, and a frequency of 195.101THz. A germanium detector is connected to a power meter calibrated to 1550nm and is attached to the other end of the polarization controller to measure the optical power using an FC-APC fiber patch cord. The controller is aligned for the maximum throughput. Then LaserT is tuned to match the optical power and frequency of LaserF and connected to another polarization controller. Again, the controller is tuned to achieve the maximum possible optical power using a fiber patch cable. Changes to LaserT's power may be necessary to match the power of LaserF. The detector is disconnected from the polarization controllers and the two controllers connect to the input of a single mode fiber coupler. The detector is attached to the output of the coupler and each laser is tested individually to ensure the power is equal and to record power loss. Then the coupler is attached to an in-line single mode polarizer designed for 1550nm and again the power of each laser is checked individually for maximum modulation efficiency. Once the base system has been calibrated, it is not calibrated again and all components remain fixed and untouched. When the optical power is recorded in measurements, it is the power after the polarizer that is remeasured.

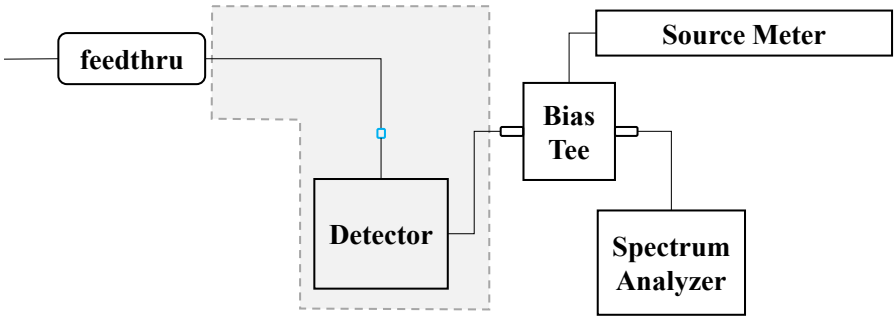

Figure 4.2 Experimental Setup for photodetector

Another fundamental setup of the experiment is the photodetector setup. The photodetector used is an InGaAs cryo-hardened 35 GHz MUTC Photodiode, meaning it is designed and packaged to be operated at room temperature and ultra-cold temperatures. Throughout numerous experiments, the photodetector connections do not change; the photodetector resides inside the cryostat regardless of test temperature and experiment. A FC-UPC patch cord connects the polarizer to the input of a fiber feedthrough, used to connect the inside of the cryostat to the outside. Inside the cryostat, the feedthrough is connected to the photodiode with another patch cord. The output of the detector connects to a SMA cable leading to sealed port which allows connection outside the cryostat. Connected to the sealed port on the outside of the cryostat is a bias tee, which takes a DC bias voltage from a source meter and sends the RF signal to a spectrum analyzer. The equipment after the base system but before the cryostat will change depending on the desired experiment, but the configuration inside the cryostat does not move or change

A vector network analyzer is connected to the SMA cable at port 1 and the bias tee to measure system response this part of the system. The reflection signals, S11 and S22, are recorded over a large frequency range to observe the limitations of the components used. The transmission signals, S12 and S21, are also recorded to observe loss and limitations of

components. In the results section, this baseline measurement is removed from the final report of the frequency response. This measurement is only done once, or more if the experimental setup of the photodetector changes.

The experimental procedures described below are used for both room temperature experiments and cold temperature experiments. For cold temperature experiments, the cryostat is pumped until a pressure of 0.00074mbar at least is reached. Then liquid nitrogen is added to the cryostat until full and the temperature sensor reads 78K. To ensure the photodetector is also cooled to 78K, the experiment will not start until at least 30 minutes have passed since the nitrogen has been added to ensure thermal equilibrium. Then throughout the experiment more nitrogen is added as needed.

4.2 Photodiode Characterization

When first receiving a photodetector, it is important to first measure the dark current and responsivity to test the validity of future measurements and monitor degradation over time. This experiment is done as soon as the photodetector is received and repeated over time to monitor the properties of the photodiode.

For the dark current measurement, both lasers are connected to the system but are not operational. The polarizer is connected directly to the fiber feedthrough and the bias tee is disconnected from the spectrum analyzer. A measurement program for the source meter called TSP Express is used to sweep the bias voltage from +0.5V to -5V and record the current vs. bias voltage. The log of the current vs. bias voltage is then used as the standard. These results are compared over time to ensure the device does not have a high dark current and does not show signs of degradation. Dark current is recorded at room temperature and 80K.

Responsivity of the photodetector is measured by dividing the photocurrent by the input optical power. LaserF remains off and LaserT is held at a constant power but swept through its frequency range, 191.5THz – 196.5THz, in steps of 0.5THz. The optical power is measured after the polarizer using the germanium detector for each frequency step. Then the polarizer is connected to the fiber feedthrough and LaserT is again swept through its frequency range while the source meter measurement program records the current. The current is divided by the optical power which gives the responsivity at each frequency. Responsivity is recorded and compared at room temperature and 80K.

4.3 Frequency Response Measurement Setup and Procedure

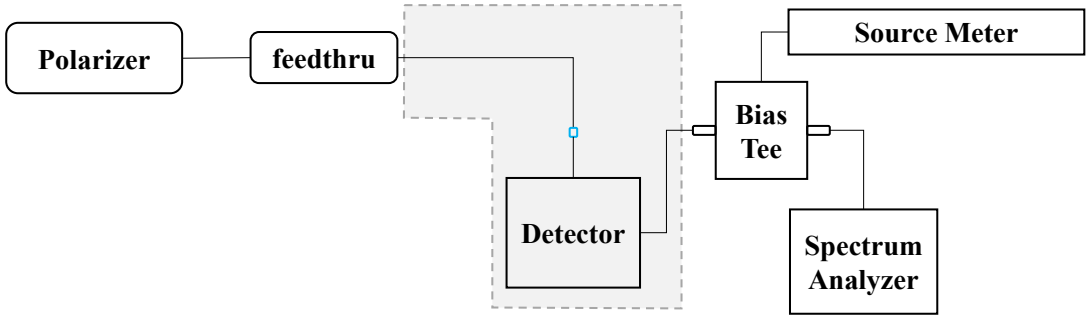

Figure 4.3 Experimental setup for frequency response measurement

The frequency response measurement shows the available bandwidth of the photodiode. These results show what frequencies are suitable for this device and system without large power losses. The frequency response of a device is affected by the capability of the device and the components in the system. Certain components have frequency limitations which can cause a decrease in the RF power at these frequency limits. The spectrum analyzer observes the amplitude across a range of frequencies, in this case from 0GHz to 27GHz.

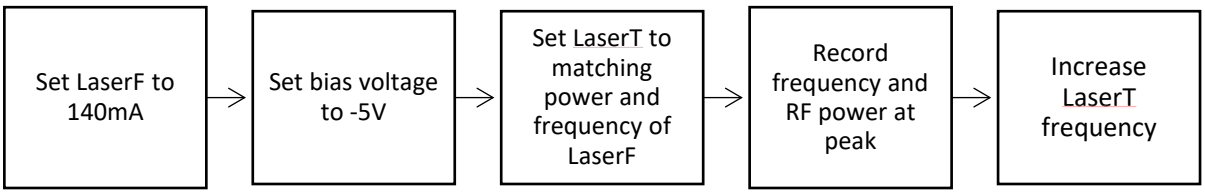

Figure 4.4 Frequency response measurement procedure

The procedure for the frequency response measurement is shown in Figure 4.4. First, LaserF is set to 140mA and the power is recorded with the germanium detector connected to the polarizer. Then LaserT is set to 195.101THz and the power is matched to LaserF. After the power of each laser individually and the combined power is recorded, the germanium detector is disconnected and the polarizer is connected to the fiber feedthrough using a patch cord. The current of each laser individually and the combined current is recorded from the source meter at a reverse bias voltage of 5V. LaserF is set to 140mA and remains on during the entire experiment. A bias voltage of -5V is set on the source meter and remains on the for the experiment. LaserT is set to the matching optical power of LaserF and starts at 195.100THz. Once the laser has stabilized, the frequency and RF power of the peak on the spectrum analyzer is recorded. LaserT is then set to a frequency of 195.098THz and again the frequency and RF power from the peak on the spectrum analyzer is recorded. The process of changing the frequency of LaserT and recording the data from the peak is repeated in steps of 2GHz for the range of the spectrum analyzer used, typically 27GHz. This procedure is followed at room temperature and cold temperature.

4.4 Linearity Measurement Procedure

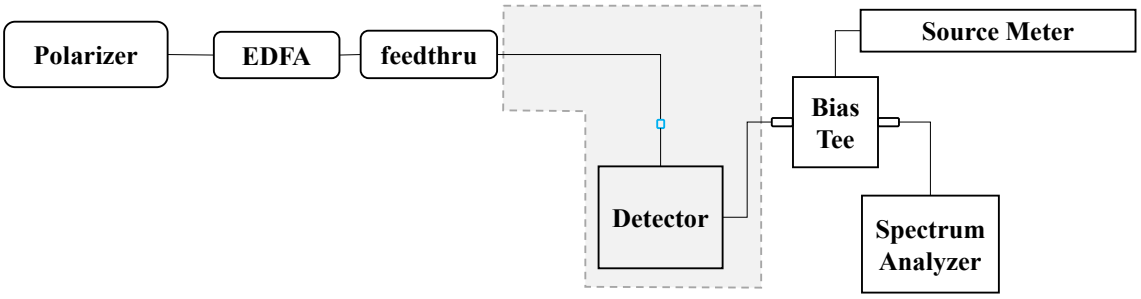

Figure 4.5 Experimental setup for linearity measurement

The linearity of a photodiode is an important parameter for accurate electrical response and to minimize harmonic signal distortion. Outside the range of linearity, the results become inefficient and unreliable. This experiment setup is similar to the frequency response measurement system but utilizes an EDFA to change the input power. It can amplify the power up to 20dB by user control of the current. Not only is the current of the EDFA changed, but two frequencies of 3GHz and 10GHz are measured. Also, two reverse bias voltages of 0V and -5V are explored. That means each bias voltage is tested with both frequencies, and each frequency sweeps the EDFA current from 200mA to 1000mA.

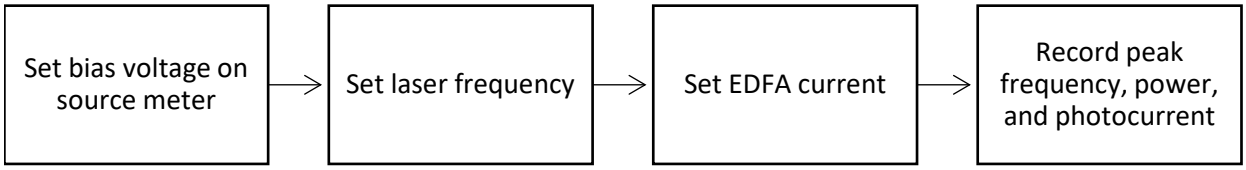

Figure 4.6 Linearity measurement procedure

The procedure for the linearity measurement is shown in Figure 4.6. First, LaserF is set to 80mA and the power is measured using the Ge detector connected to the polarizer. Then LaserT is set to 195.123THz, the matching frequency of LaserF, and the power is tuned until it is equal to the optical power of LaserF. Power of the individual lasers and the lasers combined are recorded. LaserF will remain on during the experiment and LaserT will change frequencies but remain at the observed power. The Germanium detector is disconnected and the polarizer is connected to the input port of the EDFA. The output port is connected to the Germanium detector to measure the power through the EDFA. With a starting current of 200mA and a target temperature of 25°C, the EDFA current is increased in steps of 25mA and the power is recorded at each step. Since this high power can damage the photodiode if it is outside the linear region, a maximum power of 50mW is commonly used when measuring for repeatability. To test the full scope of linearity region, the full capability of the EDFA is used. The Germanium detector is disconnected and the output port is connected to the fiber feedthrough using a patch cord. The initial settings for the first experiment are as follows: bias voltage of -5V, LaserT frequency of 195.126THz for a final frequency difference of 3GHz, and EDFA current of 200mA. At the lowest level of the procedure, the EDFA is increased in steps of 25mA all the way to the maximum power for that day, typically 500mA or the full 1000mA. Once the EDFA is set, the frequency and power of the peak observed on the spectrum analyzer is recorded along with the photocurrent. Then the EDFA current is increased and the frequency, power, and photocurrent are recorded. At the end of the EDFA current sweep, the EDFA is slowly reset to 200mA and the frequency of LaserT is increased to 195.133THz, for a final frequency difference of 10GHz on the spectrum analyzer. The EDFA is then swept again while recording the frequency, power, and photocurrent at each step. Once the 10GHz measurement is completed at -5V, the procedure is

repeated for 0V bias. LaserT is set to 195.126THz, the EDFA is swept, and the frequency, power, and photocurrent are recorded at each step. Then LaserT is set to 195.133THz and the EDFA is swept again. This results in two bias voltages of -5V and 0V, two frequencies of 3GHz and 10GHz, and 32 total EDFA steps with a range of 200mA to 1000mA. The measurement is completed at room temperature and 80K.

4.5 Automated Measurement Programs

Each experiment is very simple in concept, but the interaction with all the different instruments can be time consuming and repetitive. Also, the signal is not completely stable. Since there is slight variation in power and polarization, 100% modulation efficiency is not always achieved. There is partial destructive interference observed in the spectrum analyzer waveform, so the peak will shift slightly left and right and up and down. This change is only a couple dBm's, but only the data at 100% modulation efficiency is desired. To combat the interactions with multiple instruments and the small instability in the measurement results, automated programs have been written that follow the measurement procedures in MATLAB and in LabVIEW.

Each measurement in LabVIEW functions as a finite state machine. VISA resource is used to connect to each instrument, but each instrument connects differently to the computer. The EDFA and LaserT connect using USB, but the source meter and the spectrum analyzer connect using ethernet. While there are no errors, an initial command is sent into a while-loop with a case statement inside. This command determines which task the case statement will perform. Once the task is complete, another command is sent into the while-loop using a shift register, and the process repeats or changes depending on the desired measurement.

4.5.1 Frequency Response Automated Program

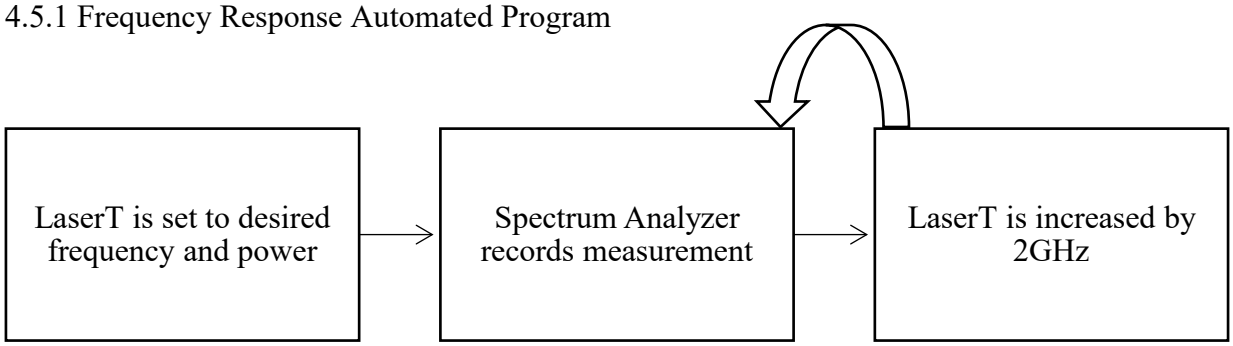

Figure 4.7 Frequency response automated program flow

The program flow for the frequency response measurement is shown above in Figure 4.7. Outside of the LabVIEW program, the user only needs to turn on LaserF to 140mA. To create a finite state machine functionality in LabVIEW, the outer structure is a case structure that checks for errors in the program. Then a for-loop runs and the number of iterations is determined by the frequency range of the spectrum analyzer and the LaserT frequency increments. For a 26GHz analyzer and a frequency step of 2GHz, the loop will run 14 times. Inside the for-loop is a while-loop that runs for as long as there are repeatable tasks. A case structure is inside to determine what task will be completed, then the programming and sub-VIs are placed inside the corresponding task.

The user sets the parameters in the front panel then starts the program. The source meter is turned on the bias voltage and limit set by the user, completed outside all structures. First, the "Start Laser" command is sent into the for-loop. LaserT connects through serial USB port and receives data packets. A command is written with a data packet that includes a checksum, an indicator for read or write, the register that indicates the parameter (power, frequency, etc.), and the value to be sent, all in hexadecimal. The command to set the power and frequency, determined by the user, are written and a 90 second delay is added so the laser can warm up. In

this stage, a status register on the front panel reads “Starting Laser”. Once the laser is warmed up, this task sends the next command, “Take Measurement”. Inside this task, the spectrum analyzer uses SCPI commands to set basic parameters such as frequency range, reference level, and attenuation input by the user. Connected to the computer via ethernet, the analyzer will then begin a maximum hold function, meaning it reads data for a specified period but only saves the maximum value at each point. This allows the data to be recorded when 100% modulation efficiency occurs. The status register will read “Taking Measurements” during this task. Next, the laser is turned off, and the while-loop is exited. The frequency of LaserT is increased outside the for-loop and the while-loop begins again. The process will repeat: the laser is turned on, the measurement is recorded, then the frequency is increased. Once the for-loop has completed the desired number of iterations, the loop is exited and the source meter is turned off. The data is stored as a table in a CSV file.

4.5.2 Linearity Automated Program

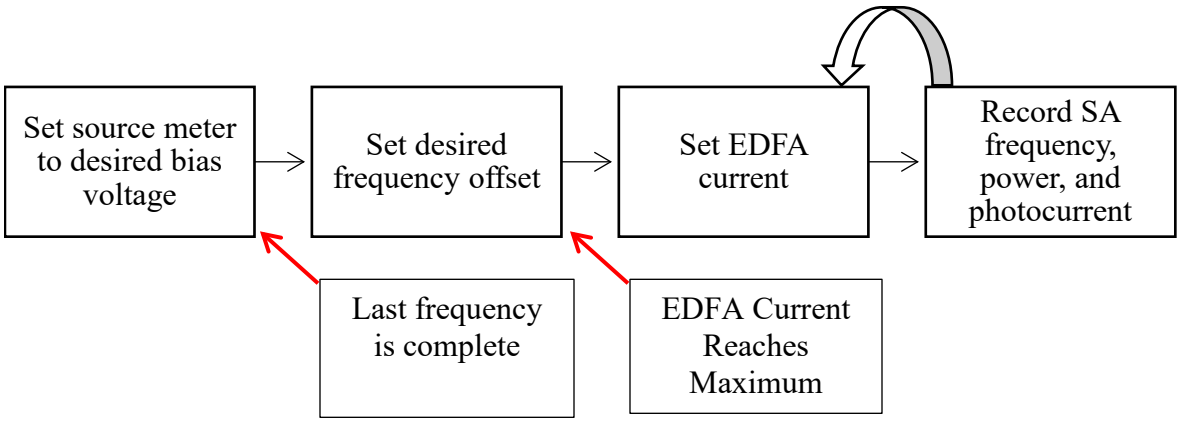

Figure 4.8 Linearity automated measurement program flow

Figure 4.8 describes the automated program flow for the linearity measurement. The user only needs to turn on the power for LaserF, the rest of the measurement is done inside the

program. Like the frequency response program, the linearity program also functions as a finite state machine. Different commands are fed into a while-loop to determine which task to perform; however, this program has two for-loops: the outer for- loop changes the bias voltage and the inner for-loop changes the frequency. Typically, two bias voltages and two frequencies are used, but the program can easily be changed to accommodate any number of voltages and frequencies.

The user will turn on LaserF, set the input parameters on the front panel, then start the program. The first command sent into the while-loop is to turn on the source meter to the desired bias voltage, typically -5V is the first, then the frequency is set to the desired offset by the user, typically the first frequency is 3GHz. Then the EDFA is set to 200mA, enabled, and the spectrum analyzer starts recording the measurement. Again, the maximum hold function is used to ensure the peak at 100% modulation efficiency is captured. Once the spectrum analyzer task has finished, the EDFA task is called again, and the current is increased by 25mA. The EDFA and spectrum analyzer task repeat until the EDFA current has reached the maximum, usually 1000mA. In this case, the frequency offset is increased to 10GHz and the EDFA is reset to 200mA. Again, the EDFA and the spectrum analyzer repeat until all measurements for this frequency have been taken. After the last frequency has completed, the bias voltage is set to 0V. The frequency offset is set back to 3GHz and the entire process repeats. When the measurements for both bias voltages and frequencies are complete, the devices will be disabled and turned off, and the data saved as a CSV file.

CHAPTER 5. RESULTS AND DISCUSSION

5.1 Dark Current

Dark current is the residual electrical current flowing through a device without illumination. Ideally, a low dark current is observed so it is negligible in the noise calculations and to indicate no signs of device degradation. Electrons and holes are accidentally generated in the depletion region of the photodiode, causing a small current, even without illumination. While the dark current can be minimized in developing the structure of the photodiode and ensuring proper heatsinking, it will still exist. Monitoring the dark current over the lifetime of the device can show signs of degradation if the noise increases.

The log of the current versus bias voltage at different temperatures are plotted to form the dark current results, as shown in Figure 5.1. The results on the left are provided by Freedom Photonics and shows a bias voltage sweep from +1V to -5V at temperatures ranging from 86K to approximately 270K. Figure 5.1b shows the experimental results for dark current at room temperature and at liquid nitrogen temperature, approximately 80K. There is a strong overlap between the dark current at room temperature and low temperature, approximately 8nA for both for an applied reverse bias voltage. Similar to the expected results, the low temperature will shift the dip and rise at positive bias voltage. The source meter used has different resolution thresholds: one at 200mV, then 2V, then 20V. This resolution threshold prevents a smooth measurement from -5V to +1V but allows a finer resolution at small bias voltages

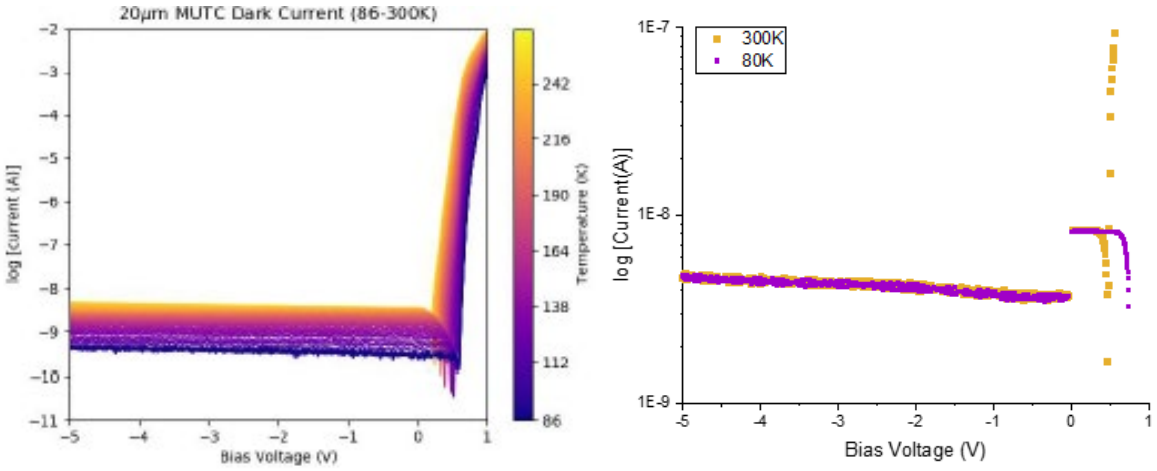

(a) (b)

Figure 5.1 Dark current expected results(a) and measurement results(b) for 300K and 80K

5.2 Responsivity

Responsivity indicates how well a diode converts incoming light into electrical current. It describes how high the output photocurrent is compared to the optical power entering the photodiode. A high responsivity is always desired, but it can be reduced by material, structure, wavelength, and especially temperature.

The responsivity is calculated by dividing the photocurrent measured at -5V bias by the optical power. A frequency tunable laser is used to sweep the laser frequency from 191.5THz to 196.5THz in steps of 0.5THz, which corresponds to a range of 1570nm to 1525nm. Responsivity for this frequency range is shown in Figure 5.2 for room temperature, 300K, and liquid nitrogen temperature, 80K.

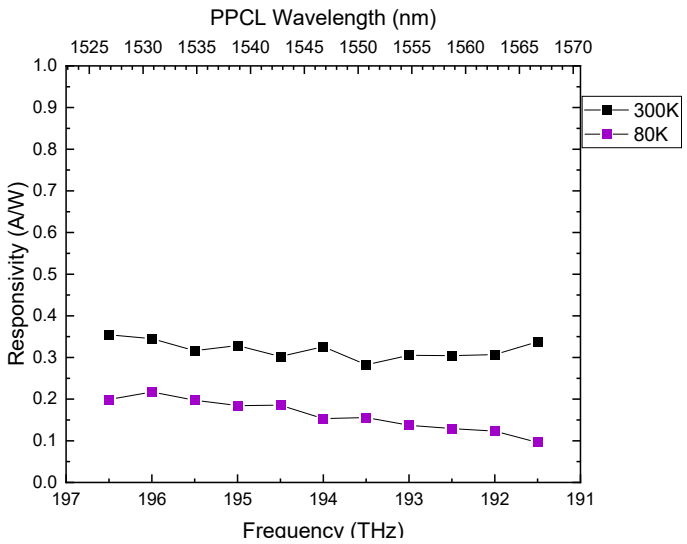

Figure 5.2 Responsivity vs. frequency and wavelength for 300K and 80K

For 1550nm at 300K, the responsivity was measured to be 0.328 A/W and at 80K it was measured to be 0.184 A/W. The reduction in responsivity at low temperatures can be attributed to an increase in band gap with lower temperatures. At colder temperatures, it takes more energy to excite an electron, therefore resulting in shorter response time and lower responsivity. Since responsivity and quantum efficiency are closely related, quantum efficiency can be calculated using the measured responsivity and known wavelength. With a center wavelength of 1536 nm and a responsivity of 0.35 A/W, the quantum efficiency is calculated to be 28%.

5.3 System Response

The system response measures the device under test for a range of frequencies. A vector network analyzer can identify scattering parameters across this range of frequencies as well as providing calibration for these components. This observes the power ratio transferred between two ports for a given network. In this case, we observe the system after the photodiode and

before the spectrum analyzer, including: SMA cables, adapters, and the bias tee. The transmission(S21) and reflection(S11) are shown in Figure 5.3.

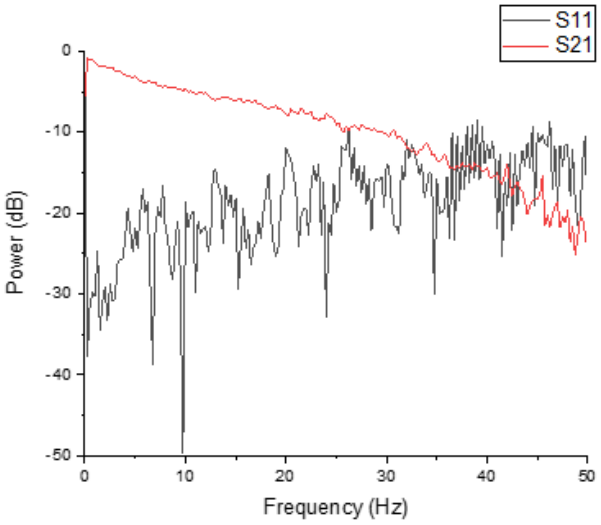

Figure 5.3 System response showing S11 and S12

Scattering parameter S11 shows the reflection of the signal back to the input, or the return loss. This can be due to impedance mismatch or Fresnel reflections, which can occur at the end of optical fibers. Loss and reflection increase with the number of connectors used due to the free space in the connectors. This system tested includes two SMA cables, 3 connectors, and the bias tee. Also, components and cables have a recommended frequency limit for best results. SMA connectors and cables typically reach a maximum around 22GHz, which can also attribute to the high reflection and loss at high frequencies.

5.4 Frequency Response

Frequency response describes the bandwidth of the photodetector, meaning it displays the speed of the photodetector using RF power and frequency. The bandwidth is determined by the electrical parameters, such as capacitance and resistance, but also by internal factors such as the transit time inside the depletion region. There are many tradeoffs when considering this parameter including active area size, allowed photocurrent, and dark current.

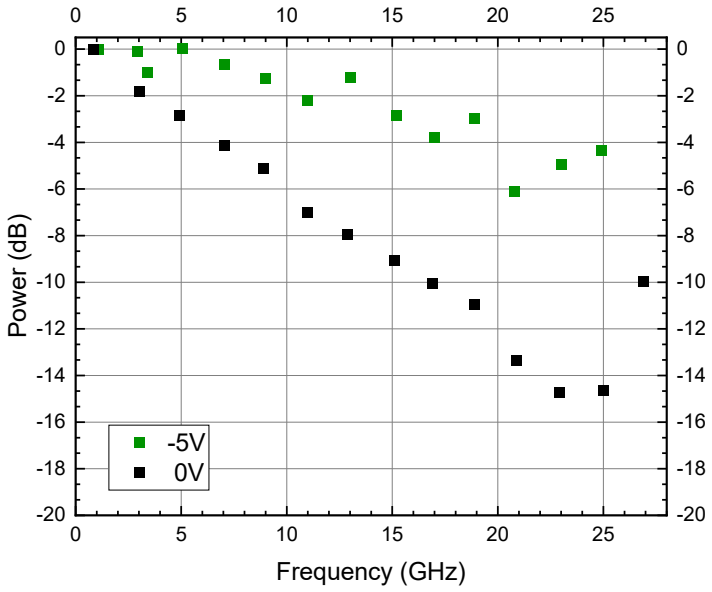

Figure 5.4 Frequency response of MUTC-PD with -5V and 0V voltage bias

The results shown in Figure 5.4 have the system response subtracted and measurements normalized to the smallest frequency and has an input optical power of 11.75mW. At 300K -5V bias, the 3dB bandwidth is 18.9GHz whereas at 0V bias the 3dB bandwidth is approximately 6GHz. Figure 5.5 shows the results at 80K. No 3dB bandwidth is reported due to these results being recorded without the automated measurement program in LabVIEW, but it demonstrates

the relationship with photodiode bandwidth and temperature. Even with the same input optical power and temperature, -5V applied bias voltage shows higher response than the 0V applied bias voltage.

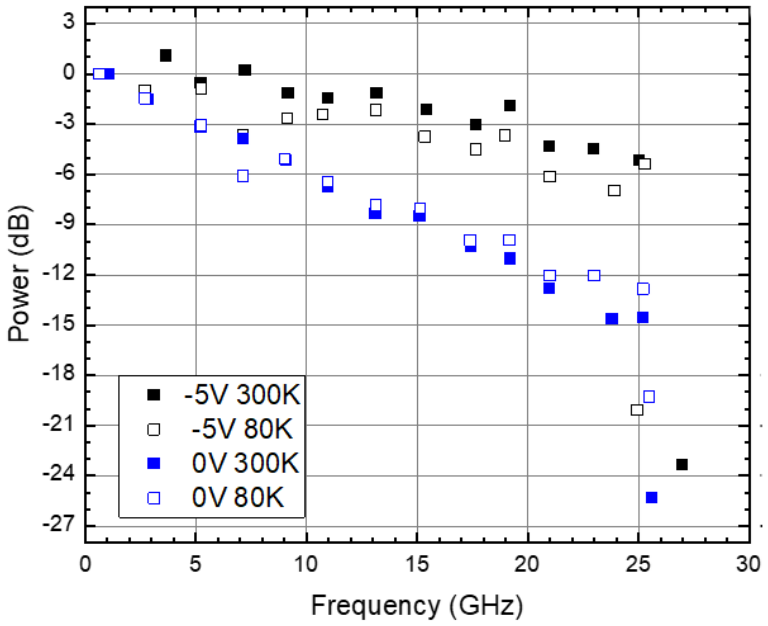

Figure 5.5 Frequency response at -5V and 0V applied bias at 300K and 80K

Figure 5.6 can help describe why a higher reverse bias shows higher frequency response than the 0V bias voltage measurements. Figure 5.6(left) shows the measurement trace for a frequency of 3GHz and a bias voltage of -5V. Figure 5.6(right) shows the measurement trace for a frequency offset of 3GHz and an applied bias voltage of 0V. Without bias voltage, more harmonics are shown, which use power that cannot be used by the beating of the two lasers, the peak shown. Harmonic distortion is unfavored because it results in power loss from the desired signal.

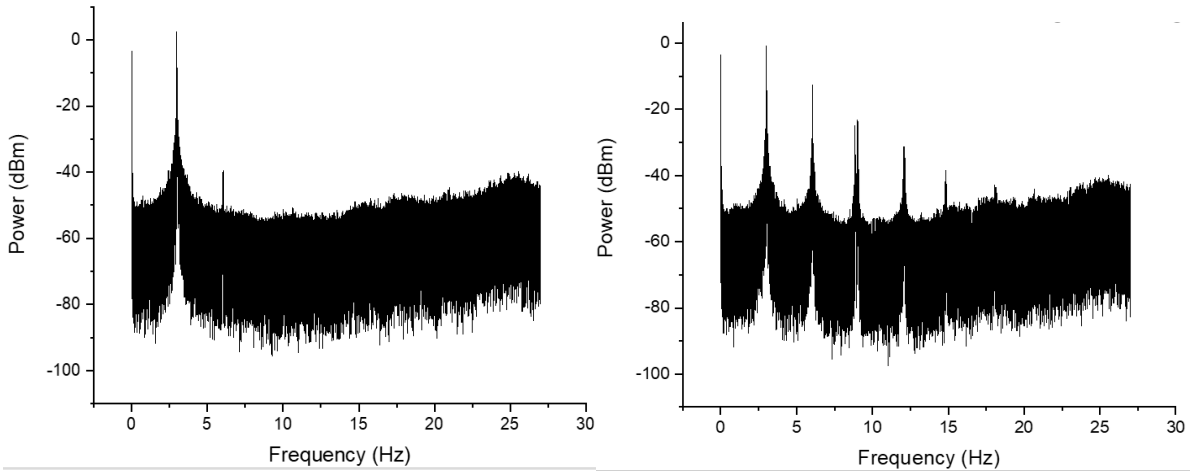

Figure 5.6 Harmonic distortion found in 3GHz offset for -5V(left) and 0V(right)

Frequency response results demonstrate the -5V applied bias has a higher 3dB bandwidth than no applied bias at room temperature and cold temperatures of 80K. It also shows that without bias voltage, there are harmonic distortions that can take away from the power of the combined signals.

5.5 Linearity

A photodiode operating in the linear region means that photocurrent increases linearly with input optical power. Operating in this region is important to ensure accurate electrical response. Outside of the linear region, the saturation current is found and the response becomes unpredictable.

The results for the linearity measurements are shown in Figure. 5.7 at room temperature. Figure 5.7a shows the raw measurement data for two bias voltages of -5V and 0V and two frequencies of 3GHz and 10GHz. The same parameters are shown in Figure 5.7b but instead with the compression curve form. This curve derives from the difference between a polynomial

fit of the raw data in Figure 5.7a compared to the ideal response. As shown, a bias voltage of -5V for both frequencies do not reach a plateau, so the saturation current and 1dB compression point is above 45mA; however, a plateau and drop-off are shown for the 0V measurements. At 3GHz the 1dB compression point is estimated to be approximately 18mA and for 10GHz the approximate 1dB compression point is about 24mA. A confident 1dB compression point is not reported due to the difficult with fitting for the raw data. In these results, a 5th order polynomial was used for the 0V results and a 3rd order polynomial fit is used for -5V bias voltage. Although polynomial is not the exact fitting for this data, it was used for convenience and to demonstrate the clear difference between the two bias voltages.

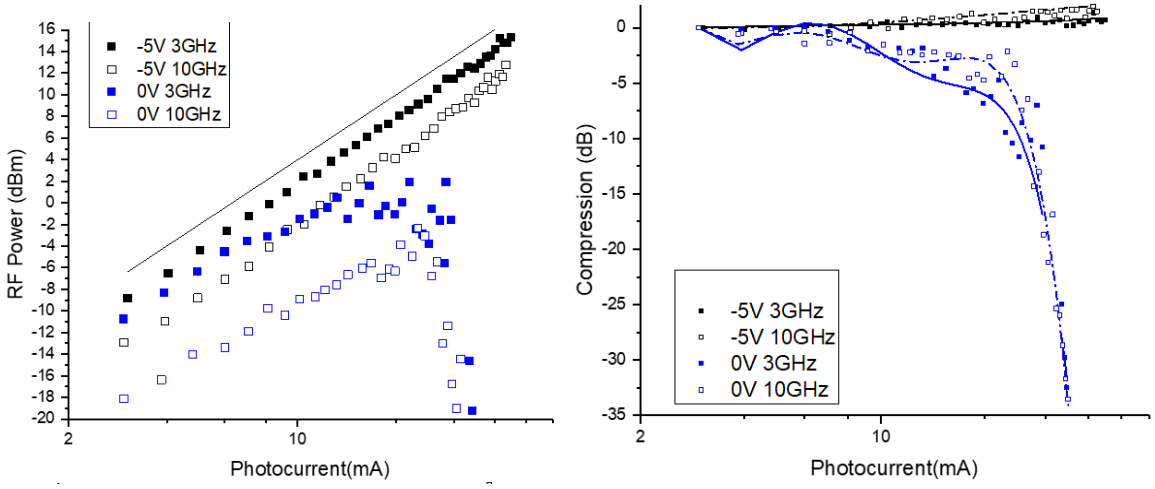

(a) (b)

Figure 5.7 Linearity results(a) and compression curve(b) at 300K

The results for the linearity measurement at 80K are shown in Figure 5.8. A compression curve is a great tool for determining the 1dB compression point; however, finding an appropriate fit for the 0V results has been difficult, so a polynomial 5th order polynomial fit is used for those

results and the 1dB compression point is estimated from the raw data. For both frequencies at -5V bias, a compression is not seen, so the 1dB compression point is above 25mA for a temperature of 80K. Estimating the 1dB compression point for the 0V data is difficult, but for 3GHz the approximate point is 14mA. The 1dB compression point is larger for 10GHz at approximately 20mA.

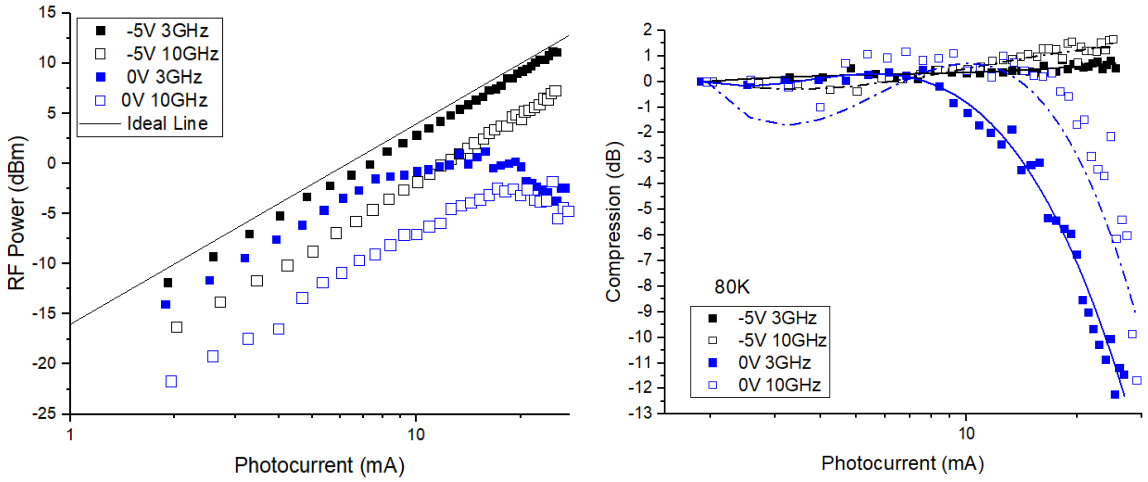

Figure 5.8 Linearity results for 80K

Table 5.1 summarizes the results for linearity measurement at -5V bias and 0V bias with frequencies of 3GHz and 10GHz and at temperatures of 300K and 80K. All measurements were taking with an input optical power of 5.42mW of combined laser power. The reduction in compression points at lower temperatures compared to higher temperatures could be attributed to the decrease in responsivity at these temperatures. These results also show one benefit of applied bias voltage: a larger 1dB compression point and larger saturation current.

Table 5.1 Linearity measurement results summary

	1dB @ 300K	**1dB @ 80K**
-5V 3GHz	> 45mA	> 30mA
-5V 10GHz	> 45mA	> 30mA
0V 3GHz	~ 18mA	~ 14mA
0V 10GHz	~ 24mA	~ 20mA

CHAPTER 6. CONCLUSION AND FUTURE WORK

Researching and fabricating devices that can handle the current environmental restraints is challenging but trying to find solutions to these limitations can provide insight into potential solutions for bringing quantum computers into common households. Measuring the bandwidth of a modified uni-traveling carrier photodiode can shed light into the possibilities of higher frequency usage in quantum computers, resulting in more data being transmitted. Also, observing the dependence of linearity on frequency, bias voltage, and temperature can further show capabilities of the MUTC-PD.

A microwave photonic link using the heterodyne method with two individual light sources has been demonstrated. The MUTC-PD showed a very low dark current of approximately 8nA for room temperature and liquid nitrogen temperatures of 80K. Having an applied reverse bias voltage showed greater bandwidth, higher saturation current, higher 1dB compression point, and lower harmonic distortion than without any applied voltage bias. These results show the improvements that can be made by adding a bias tee and an applied bias voltage to this system. While results can be seen without any bias, the photodiode will be reduced to a lower frequency response and inaccurate electrical response at higher photocurrents.

These investigations of a modified uni-traveling carrier photodiode can provide insight and possible improvements to already existing systems for testing quantum internet applications. Many researchers are working to improve currents systems as well as investigate other parameters and solutions. A research group at NIST explored the scalability of qubits as well as

the noise found in photonic links. The results showed they were able to scale qubits and photonic link was limited by the shot noise, so it is a great option for quantum information applications over the traditional coaxial cable [37]. Oak Ridge National Lab has developed the first adaptive bandwidth provisioning for entanglement in deployed local quantum network. These researchers demonstrated remote state preparation at over three nodes in all three locations on the campus. Successful entanglement distribution was found for two allocations of eight dynamically reconfigurable channels [38,39,40].

In the nearby future, this system will be tested using a dilution refrigerator located at Oak Ridge National Laboratory. These results will hopefully provide a clear comparison with other systems operating at ultra-low temperatures and test the detector for its temperature capabilities. The heterodyne method will be used to create a microwave signal for the MUTC-PD, which will be cooled down to approximately 2K. The measurements performed in this thesis will be repeated at this low temperature to further demonstrate the temperature dependencies of frequency response and linearity.

REFERENCES

[1] "History of Telecommunication." Accessed March 17, 2022. https://www.mitel.com/articles/history-telecommunication.

[2] Arumugam, M. "Optical Fiber Communication—an Overview." *Pramana* 57, no. 5-6 (2001): 849–869.

[3] Gambling, W.A. "The Rise and Rise of Optical Fibers." *IEEE Journal of Selected Topics in Quantum Electronics* 6, no. 6 (2000): 1084–1093.

[4] "The History of Coaxial Cable." *QRZ NOW - Ham Radio News*. Last modified December 16, 2015. Accessed March 30, 2022. https://qrznow.com/the-history-of-coaxial-cable/).

[5] "Why Coaxial Cables Are Highly Insulated ...???" *Why Coaxial Cables Are Highly Insulated ...???* Accessed May 9, 2022. https://onebyzeroelectronics.blogspot.com/2015/05/why-coaxial-cables-are-highly-insulated.html.

[6] "Optical Fibers." *Optical Fibers*. Accessed May 1, 2022. http://labman.phys.utk.edu/phys222core/modules/m7/optical-fibers.html#:~:text=An%20optical%20fiber%20consists%20of,carrying%20portion%20of%20the%20fiber.

[7] Learning Chemistry. "Optical Fiber - Cable, Definition, Properties, Types, Uses." *Learning Chemistry*. Last modified December 27, 2021. Accessed March 22, 2022. https://www.priyamstudycentre.com/2021/07/optical-fiber.html.

[8] English, Jennifer. "What Is Fiber Optics? ." *SearchNetworking*. TechTarget, October 7, 2021. Last modified October 7, 2021. Accessed March 22, 2022. https://www.techtarget.com/searchnetworking/definition/fiber-optics-optical-fiber.

[9] "Fiber-Optic Cable vs. Coaxial Cable... Which Is Better?" *Chariton Valley*. Last modified May 27, 2022. Accessed March 22, 2022. https://www.cvalley.net/fiber-optic-cable-vs-coaxial-cable-which-is-better/.

[10] Urick, V. J., Keith J. Williams, Jason D. McKinney, and Vincent J. Urick. *Fundamentals of Microwave Photonics*. Somerset: Wiley, 2015.

[11] “Microwaves and Application Areas – Microwave Road.” *Microwave Road - Microwave Road*. Accessed March 20, 2022. https://microwaveroad.se/microwaves-and-application-areas/.

[12] Al-Amri, Mohammad D., Mohamed El-Gomati, and M. Suhail Zubairy. *Optics in Our Time*. Cham: Springer International Publishing, 2018.

[13] Yao, Jianping. “Microwave Photonics.” *Journal of Lightwave Technology* 27, no. 3 (2009): 314–335.

[14] Kittlaus, Eric A., Danny Eliyahu, Setareh Ganji, Skip Williams, Andrey B. Matsko, Ken B. Cooper, and Siamak Forouhar. “A Low-Noise Photonic Heterodyne Synthesizer and Its Application to Millimeter-Wave Radar.” *Nature Communications* 12, no. 1 (2021).

[15] Giraldo, Marcela. “Measurement of the Linewidth of a Laser Diode by Using the Delayed Self-Heterodyne Technique.” *Applied Optics* (May 2016).

[16] Kittlaus, Eric A., Danny Eliyahu, Setareh Ganji, Skip Williams, Andrey B. Matsko, Ken B. Cooper, and Siamak Forouhar. “A Low-Noise Photonic Heterodyne Synthesizer and Its Application to Millimeter-Wave Radar.” *Nature Communications* 12, no. 1 (2021).

[17] Paschotta, Dr. Rüdiger. “Fiber Polarization Controllers.” *Fiber Polarization Controllers, Explained by RP Photonics Encyclopedia; Bat Ear*. RP Photonics AG, July 17, 2021. Last modified July 17, 2021. Accessed February 26, 2022. https://www.rp-photonics.com/fiber_polarization_controllers.html.

[18] “Introduction to Polarized Light.” *Nikon's MicroscopyU*. Accessed March 13, 2022. https://www.microscopyu.com/techniques/polarized-light/introduction-to-polarized-light.

[19] Ethw. “Diode.” *ETHW*. ETHW, April 12, 2017. Last modified April 12, 2017. Accessed April 2, 2022. https://ethw.org/Diode.

[20] “Semiconductor Basics & Semiconductor Physics Tutorial.” *Basic Electronics Tutorials*. Last modified February 20, 2019. Accessed February 1, 2022. https://www.electronics-tutorials.ws/diode/diode_1.html.

[21] Paschotta, Dr. Rüdiger. “Fiber Polarization Controllers.” *Fiber Polarization Controllers, Explained by RP Photonics Encyclopedia; Bat Ear*. RP Photonics AG, July 17, 2021. Last modified July 17, 2021. Accessed February 26, 2022. https://www.rp-photonics.com/fiber_polarization_controllers.html.

[22] Nascimento, Luciano Nascimento, Lourdes Cristina Jamshidi, Celmy Maria Barbosa, and Reza Jamshidi Rodbari. “Semiconductors of Crystallin Alloys in Superlattices.” *Revista Tecnológica* 24, no. 1 (2015): 81–93.

[23] Liguang Zheng, Xiong Zhang, Yuping Zeng, S.R. Tatavarti, S.P. Watkins, C.R. Bolognesi, S. Demiguel, and J.C. Campbell. “Demonstration of High-Speed Staggered Lineup GAASSB-INP UNITRAVELING Carrier Photodiodes.” *IEEE Photonics Technology Letters* 17, no. 3 (2005): 651–653.

[24] “Photodiode Characteristics and Applications - OSI Optoelectronics.” Accessed April 23, 2022. http://www.osioptoelectronics.com/application-notes/AN-Photodiode-Parameters-and-Characteristics.pdf.

[25] Yoshino, K., Y. Muramoto, T. Furuta, and H. Ito. “High-Speed Uni-Travelling-Carrier Photodiode Module for Ultra-Low Temperature Operation.” *Electronics Letters* 41, no. 18 (2005): 1030.

[26] “PIN Photodetector Characteristics for Optical Fiber Communication.” *Fosco Connect*. Accessed May 30, 2022. https://www.fiberoptics4sale.com/blogs/archive-posts/95046662-pin-photodetector-characteristics-for-optical-fiber-communication.

[27] Beling, Andreas, Xiaojun Xie, and Joe C. Campbell. “High-Power, High-Linearity Photodiodes.” *Optica* 3, no. 3 (2016): 328.

[28] Team, Editorial. “Everything RF.” *What Is P1dB? - Everything RF*. everything RF https://www.everythingrf.com https://cdn.everythingrf.com/logo.png 236 48, July 23, 2018. Last modified July 23, 2018. Accessed May 30, 2022. https://www.everythingrf.com/community/what-is-p1db#:~:text=The%201%20dB%20compression%20point,distortion%2C%20harmonics%20and%20intermodulation%20products.

[29] Williams, K.J., and R.D. Esman. “Design Considerations for High-Current Photodetectors.” *Journal of Lightwave Technology* 17, no. 8 (1999): 1443–1454.

[30] “Temperature Electronics.” *Extreme*. Accessed May 12, 2022. http://www.extremetemperatureelectronics.com/tutorial3.html.

[31] Ito, H., S. Kodama, Y. Muramoto, T. Furuta, T. Nagatsuma, and T. Ishibashi. “High-Speed and High-Output INP–InGaAs Unitraveling-Carrier Photodiodes.” *IEEE Journal of Selected Topics in Quantum Electronics* 10, no. 4 (2004): 709–727.

[32] Nagatsuma, T., H. Ito, and T. Ishibashi. “High-Power RF Photodiodes and Their Applications.” *Laser & Photonics Review* 3, no. 1-2 (2009): 123–137.

[33] Ito, Hiroshi, Tadao Nagatsuma, and Tadao Ishibashi. “Uni-Traveling-Carrier Photodiodes for High-Speed Detection and Broadband Sensing.” *SPIE Proceedings* (2007).

[34] Sun, Keye, and Andreas Beling. “High-Speed Photodetectors for Microwave Photonics.” *Applied Sciences* 9, no. 4 (2019): 623.

[35] Beling, A., J. C. Campbell, K. Li, Q. Li, M. E. Woodson, X. Xie, and Z. Yang. “High-Power Photodiodes for Analog Applications.” *Microwave Photonics (MWP) and the 2014 9th Asia-Pacific Microwave Photonics Conference (APMP) 2014 International Topical Meeting on* (2014).

[36] Chtioui, Mourad, Francois Lelarge, Alain Enard, Frederic Pommereau, Daniele Carpentier, Alexandre Marceaux, Frédéric van Dijk, and Mohand Achouche. “High Responsivity and High Power UTC and MUTC Gainas-INP Photodiodes.” *IEEE Photonics Technology Letters* 24, no. 4 (2012): 318–320.

[37] Lecocq, F., J. Aumentado, S. A. Diddams, F. J. Quinlan, and J. D. Teufel. “Control and Readout of a Superconducting Qubit Using a Cryogenic Photonic Link.” *OSA Quantum 2.0 Conference* (2020).

[38] Alshowkan, Muneer, Brian P. Williams, Philip G. Evans, Nageswara S. Rao, Emma M. Simmerman, Navin B. Lingaraju, Hsuan-Hao Lu, Andrew M. Weiner, Nicholas A. Peters, and Joseph M. Lukens. “A Reconfigurable Quantum Local Area Network over Deployed Fiber.” *Conference on Lasers and Electro-Optics* (2021).

[39] Alshowkan, Muneer, Philip G. Evans, Brian P. Williams, Nageswara S. Rao, Claire E. Marvinney, Yun-Yi Pai, Benjamin J. Lawrie, Nicholas A. Peters, and Joseph M. Lukens. “Advanced Architectures for High-Performance Quantum Networking.” *Journal of Optical Communications and Networking* 14, no. 6 (2022): 493.

[40] Alshowkan, Muneer, Nageswara S. Rao, Joseph C. Chapman, Brian P. Williams, Philip G. Evans, Raphael C. Pooser, Joseph M. Lukens, and Nicholas A. Peters. “Lessons Learned on the Interface between Quantum and Conventional Networking.” *Driving Scientific and Engineering Discoveries Through the Integration of Experiment, Big Data, and Modeling and Simulation* (2022): 262–279.